Received: 19 July 2021 | Revised: 18 February 2022 | Accepted: 27 July 2022

DOI: 10.1002/mma.8633

RESEARCH ARTICLE

WILEY

A study about the solution of convection–diffusion–reaction equation with Danckwerts boundary conditions by analytical, method of lines and Crank–Nicholson techniques

Lucía Agud Albesa[1] | **Macarena Boix García**[1] | **M. Leonor Pla Ferrando**[1] | **Salvador Cayetano Cardona Navarrete**[2]

[1]Applied Mathematics Department, Universitat Politècnica de València, Valencia, Spain

[2]Chemical and Nuclear Engineering Department, Universitat Politècnica de València, Valencia, Spain

Correspondence
Lucía Agud Albesa, Applied Mathematics Department, Universitat Politècnica de València, Camino de Vera s/n, 46022 Valencia, Spain.
Email: lagudal@mat.upv.es

Communicated by: D. Zeidan

We compare different solutions of the convection–diffusion–reaction problem with Danckwerts boundary conditions. Analytical solution is found, and method of lines and Crank–Nicholson method are described, applied, and compared for different values of *Péclet* and *Damköhler* numbers. The eigenvalues and eigenfunctions have been obtained for all the possible values of the dimensionless parameters. And the analytical expression of the concentration has been calculated with the optimum number of terms in the Fourier expansion.

KEYWORDS

convection-diffusion-reaction equation, Crank–Nicholson, Danckwerts conditions, heat equation, MOL, Péclet and Damköhler numbers

MSC CLASSIFICATION

65M06, 65M22, 65M12, 68W25, 35K57, 35Q79, 42A16

1 | INTRODUCTION

The convection–diffusion–reaction equation has important applications in areas like fluid dynamics, heat or mass transfer, chemical reaction processes, and contaminant transport.[1,2] For this reason, there exists a wide literature about its resolution, numerically and analytically.[3–5]

It is known that when a Neumann condition appears, the conservation equation for concentrations in the interior of domain fails.[1] This fact produces an inconsistency with the physical problem since the conservation of the mass requires Robin conditions at the end. In the case here described the Danckwerts assumption has been considered, but that introduces an error into predicted concentrations. This error is inversely proportional to *Péclet* number called *Pe*, dimensionless parameter that measures the ratio of the characteristic diffusion time to the characteristic advection time.[5,6]

Some of the analytical techniques used for solving this equation with other initial and boundary conditions consist in converting the original equation into a heat one by changes of variable together with the boundary conditions are converted in homogeneous. This kind of problem can be solved either by separation of variables or by using a Laplace transform.[7] But when the initial and boundary conditions are complicated, the analytical solution is usually unavailable or is given by transcendental errors functions.[5] In this work, the most relevant operations has been indicated opting for the method of separation of variables.

A general description about obtaining the analytical solution is done in Golz and Dorroh[1] taking Robin boundary conditions, and lastly, the boundary condition at the end is modified to Neumann type. Then, the produced error above mentioned is studied. But there is no existing detailed description about how to find the analytical solution and the eigenvalues when the Neumann condition is considered. In that paper, only the verified relation and a quote over the asymptotic behavior of these eigenvalues is measured, while in Jiménez Zenteno,[3] the convection–diffusion–reaction equation with Danckwerts homogeneous boundary conditions is solved. Separation variables and Fourier expansions are used, and eigenvalues and eigenfunctions are built.

One of the first objectives of this work is to develop exhaustively how to obtain the analytical solution for the convection–diffusion–reaction equation with non-homogeneous Danckwerts boundary conditions. The analytical technique detailed here is similar to the one described in the previous mentioned works; besides in this paper, the eigenvalues are also found and calculated for several values of *Péclet* and *Damköhler* numbers. This second parameter, called *Da*, measures the ratio of the characteristic diffusion time to the characteristic reaction time.[6] Both parameters are defined in the next section. The obtained eigenvalues cannot be directly calculated because a transcendental non-linear equation is satisfied. This type of equations gets involved in a wide quantity of examples.[8] For solving it, here, a numerical method has been employed.

From the numerical point of view, there are several works about how to solve different partial differential equations (PDEs) with numerical methods. In Olsen-Kettle,[9] the definition and application of a great variety of them for one- and two-dimensional heat and diffusion equations can be found; generally, the considered initial and boundary conditions are Dirichlet, Neumann, or Robin type. A brief list of some of the explained numerical methods for one-dimensional equation is as follows: explicit methods (finite differences, explicit forward Euler method, and method of lines [MOL]), implicit methods (implicit backward Euler method and Crank–Nicholson [C-N]), and iterative methods (Jacobi, Gauss–Seidel, and relaxation methods), while as for 2D equation only, it is considered the 2D finite differences.

On the other hand, it can be consulted in Vande Wouwer et al,[10] a summary about the development of Matlab-based MOL toolbox (called Matmol) in three applications: Burgers' equation in one dimension, Burgers' equation in two dimensions, and as last application, a study of benzene hydrogenation and the poisoning kinetics in a three-zone tubular reactor; this third example is a dynamic model that includes material balance equation, energy balance, and an equation that represents catalyst deactivation (in all the cases studied here, Dirichlet initial conditions and Neumann boundary conditions are taken).

Another type of examples are studied in David et al[11] where the MOL is applied to the secondary settler models with Dirichlet initial conditions and Robin type boundary conditions, parabolic PDE problem. The authors also use the previous toolbox of Matlab development by Vande Wouwer et al.[12]

There is a general study of several numerical methods in Vande Wouwer et al[2] when the 1D advection–diffusion equation with initial and boundary conditions Dirichlet type is considered. If we focus the attention on this numerical resolution, in that work, the time domain and spatial domain are discretized using different explicit and implicit schemes of finite differences. There, it is concluded that implicit methods are unconditionally stable while the explicit methods must satisfy the Von Neumann stability conditions. All these methods are compared obtaining that Crank–Nicholson, under these assumptions, has a very good behavior with respect to analytical solution.

Due to this last conclusion, in the work presented here, the comparison between MOL and Crank–Nicholson's method are studied for the 1D convection–diffusion–reaction equation with initial and Danckwerts boundary conditions. In this academic study, three different techniques of resolution are carried out. The studied problem corresponds to the variation of concentration of a solute in a tubular reactor of length L and radius R. The analytical solution obtained is compared with two numerical methods: MOL and Crank–Nicholson's method.

This paper is organized as follows. In the first section, all the involved parameters and the PDE with initial and boundary conditions are described. Following section shows the obtention of the analytical solution and the eigenvalues for several *Pe* numbers. These values cannot be found by analytical methods, and so, Table 1 just requires a numerical calculus. The solution is written by a Fourier expansion. Moreover, a `Matlab` routine has been developed for calculating and illustrating the associated concentration curves for different values of *Pe* and *Da*. These graphs show perturbations for any *Pe* and *Da* numbers. This fact became to the authors to analyze the suitable number of terms in the expansion expression. When in the literature Fourier expansions have appeared, the number optimum of terms to calculate the analytical solution by computational routine has not been taken into account. In this paper, for each of the dimensionless parameters, this number has been found and the concentration are represented with this quantity of terms.

TABLE 1 Eigenvalues λ_n with a tolerance of 10^{-15} for different values of *Péclet* number

	$Pe = 0.01$	$Pe = 0.1$	$Pe = 1$	$Pe = 10$	$Pe = 100$
n			λ_n		
0	0	0	0	0	0
1	0.099	0.314	0.960	2.284	3.020
2	3.144	3.173	3.431	4.761	6.042
3	6.284	6.299	6.438	7.463	9.066
4	9.425	9.435	9.529	10.326	12.091
5	12.567	12.574	12.645	13.286	15.120
6	15.708	15.714	15.771	16.303	18.153
7	18.850	18.854	18.902	19.355	21.189
8	21.991	21.995	22.037	22.429	24.230
9	25.133	25.136	25.172	25.519	27.275
10	28.274	28.277	28.31	28.620	30.325
11	31.416	31.419	31.448	31.728	33.380
12	34.557	34.560	34.586	34.842	36.439
13	37.699	37.701	37.726	37.961	39.503
14	40.840	40.843	40.865	41.082	42.571
15	43.982	43.984	44.005	44.207	45.644
16	47.124	47.126	47.145	47.334	48.720
17	50.265	50.267	50.285	50.463	51.800
18	53.407	53.408	53.426	53.593	54.884
19	56.548	56.550	56.566	56.724	57.972
20	59.690	59.691	59.707	59.856	61.062

On the other hand, the numerical resolution is made in Section 4 using two different methods, which are described and studied for the problem here worked. Their results are compared with the analytic solution in Section 5. It is important to realize that the size of the partition considered for each method must be taken into account to achieve similar precision in both.

Finally, Section 6 will be dedicated to the conclusions obtained in this study.

2 | PROBLEM DEFINITION

Let us consider a tubular reactor with length L where convection, diffusion, and a first-order reaction of the type $A \rightarrow B$ take place. Under these conditions, the process is modeled by the expression given by

$$\frac{\partial C_A}{\partial t} = -v_z \frac{\partial C_A}{\partial z} + D_A \frac{\partial^2 C_A}{\partial z^2} - k_A C_A, \tag{1}$$

where $C_A(z,t)$ is the concentration of component A along the position, z, and time, t; D_A is the diffusion coefficient of component A; v_z is the fluid velocity in z direction; and k_A is the kinetic rate constant. The following Danckwerts boundary conditions ($B.C.$) and initial conditions ($I.C.$) are considered

$$\left.\begin{array}{lll} I.C.: & C_A(z,0) = C_{A0} & \\ B.C.1: & v_z C_A(0,t) - D_A \left.\frac{\partial C_A}{\partial z}\right|_{z=0} = C_{Ae} v_z & \text{Robin type} \\ B.C.2: & \left.\frac{\partial C_A}{\partial z}\right|_{z=L} = 0 & \text{Neumann type} \end{array}\right\}, \tag{2}$$

where C_{Ae} is the concentration of component A at the reactor inlet and C_{A0} is the initial concentration along all its length. PDE described in (1) is the so-called parabolic PDE.

In order to simplify the calculus and the number of parameters of study, the variables are normalized and converted into dimensionless ones. For this purpose, the following values are considered[13]:

$$\begin{aligned} C_{An} &= \frac{C_A}{C_{Ae}} \Rightarrow 0 \leq C_{An} \leq 1, \\ Z &= \frac{z}{L} \Rightarrow 0 \leq Z \leq 1, \\ \theta &= \frac{tv_z}{L} \Rightarrow 0 \leq \theta \leq \infty, \\ Pe &= \frac{v_z L}{D_A} \ \textit{Péclet} \text{ Number.} \\ Da &= \frac{k_A L}{v_z} \ \textit{Damköhler} \text{ Number.} \end{aligned}$$

Throughout this paper, the normalized problem is formulated as

$$\left.\begin{array}{lll} & \frac{\partial C_{An}}{\partial \theta} = -\frac{\partial C_{An}}{\partial Z} + \frac{1}{Pe}\frac{\partial^2 C_{An}}{\partial Z^2} - DaC_{An} & \\ I.C. & C_{An}(Z,0) & = \frac{C_{A0}}{C_{Ae}} \\ B.C.1 & \left.\frac{\partial C_{An}}{\partial Z}\right|_{Z=0} - PeC_{An}(0,\theta) & = -Pe \\ B.C.2 & \left.\frac{\partial C_{An}}{\partial Z}\right|_{Z=1} & = 0 \end{array}\right\}. \tag{2}$$

Clearly, large *Péclet* numbers indicate a big influence of the convective term, and small *Péclet* numbers mark a bigger influence of the diffusive term in the convection–diffusion–reaction equation given in (2).

3 | ANALYTICAL RESOLUTION

The main idea of the approach here exposed is to convert this PDE into a heat equation with homogeneous boundary conditions and to carry out its resolution by, for example, separation of variables and generalized Fourier expansion.[1,3] Two changes of variable are required. The first one comes from the expression

$$C_{An}(Z,\theta) = e^{rZ-s\theta}u(Z,\theta), \tag{3}$$

where

$$r = \frac{Pe}{2}, \ \ s = \frac{Pe}{4} + Da. \tag{4}$$

These values are chosen for obtaining a heat PDE. This process can be generalized for any PDE like

$$\frac{\partial Y}{\partial t} = -A\frac{\partial Y}{\partial z} + B\frac{\partial^2 Y}{\partial z^2} - CY,$$

taking r and s as

$$r = \frac{A}{2B}, \ \ s = \frac{A^2}{4B} + C.$$

It is important to realize that the *Péclet* number verifies $Pe = 2r$. By analogy with the existing literature, we rewrite (2) as

$$\left.\begin{array}{lll} & \frac{\partial u}{\partial \theta} = \frac{1}{2r}\frac{\partial^2 u}{\partial Z^2} & \\ I.C. & u(Z,0) & = \frac{C_{A0}}{C_{Ae}}e^{-rZ} \\ B.C.1 & \left.\frac{\partial u}{\partial Z}\right|_{Z=0} - ru(0,\theta) & = -2re^{s\theta} \\ B.C.2 & \left.\frac{\partial u}{\partial Z}\right|_{Z=1} + ru(1,\theta) & = 0 \end{array}\right\}, \tag{5}$$

The problem enunciated in (5) is not homogeneous boundary condition, but the PDE is just a heat equation. For reaching homogeneous boundary conditions, the second suitable change is

$$u(Z,\theta) = v(Z,\theta) + w(Z,\theta), \tag{6}$$

where $v(Z,\theta)$ must be a polynomial function in Z of degree 1, verifying the boundary conditions of (5). From those considerations, it can be shown that

$$v(Z,\theta) = a(\theta)Z + b(\theta) = \frac{-2re^{s\theta}}{2+r}Z + \frac{2(1+r)}{2+r}e^{s\theta} = \frac{2}{2+r}(1+r-rZ)e^{s\theta}. \tag{7}$$

From (5) and taking into account (7), the following PDE is deduced:

$$\left.\begin{array}{lll} & \frac{\partial w}{\partial \theta} = \frac{1}{2r}\frac{\partial^2 w}{\partial Z^2} + G(Z,\theta) & \\ I.C. & w(Z,0) & = H(Z) \\ B.C.1 & \left.\frac{\partial w}{\partial Z}\right|_{Z=0} - rw(0,\theta) & = 0 \\ B.C.2 & \left.\frac{\partial w}{\partial Z}\right|_{Z=1} + rw(1,\theta) & = 0 \end{array}\right\}, \tag{8}$$

where

$$\begin{aligned} G(Z,\theta) &:= -\tfrac{\partial v}{\partial \theta}(Z,\theta) = -[a'(\theta)Z + b'(\theta)] = -s\tfrac{2}{2+r}\left[-rZ+1+r\right]e^{s\theta} = -sv(Z,\theta), \\ \varphi(Z) &:= \tfrac{C_{A0}}{C_{Ae}}e^{-rZ}, \\ H(Z) &:= \varphi(Z) - v(Z,0) = e^{-rZ}\tfrac{C_{A0}}{C_{Ae}} - \tfrac{2}{2+r}\left[-rZ+1+r\right]. \end{aligned}$$

It is important to realize that in this paper, $G(Z,\theta) \neq 0$, for all the values of the variables, since in problem (8), the boundary conditions are no null, and the construction of the function $v(Z,\theta)$ is assured.

In the literature, there are many references about the existence and uniqueness of the solution of this problem with Robin's conditions and Danckwerts' conditions, since in the case studied here, the coefficients are constants.[1,14–18] Due to this fact, the next subsections are directly dedicated to the construction of the analytical solution. The technique here described is the usual for these family of problems.[1,3,19]

3.1 | Resolution of the homogeneous heat equation

To solve the following homogeneous equation $\frac{\partial w}{\partial \theta} = \frac{1}{2r}\frac{\partial^2 w}{\partial Z^2}$, a solution is sought in the following way:

$$w(Z,\theta) = T(\theta)X(Z).$$

Replacing in the heat equation, it is obtained

$$X(Z)T'(\theta) = \frac{1}{2r}X''(Z)T(\theta) \iff \frac{T'(\theta)}{\frac{1}{2r}T(\theta)} = \frac{X''(Z)}{X(Z)} = \lambda.$$

It can be seen that only the case $\lambda < 0$ is possible, (Ch. 4, Vande Wouwer[20]). For convenience, it is rewritten $\lambda = -\lambda^2$. Under this assumption, the general solution of $\frac{X''(Z)}{X(Z)} = -\lambda^2$ is given by

$$X(Z) = A\cos(\lambda Z) + B\sin(\lambda Z).$$

Imposing the boundary condition $B.C.1$, the relation between constants A and B is established as follows:

$$A = \frac{B\lambda}{r}.$$

It can be taken $B = 1$, without loss of generality.

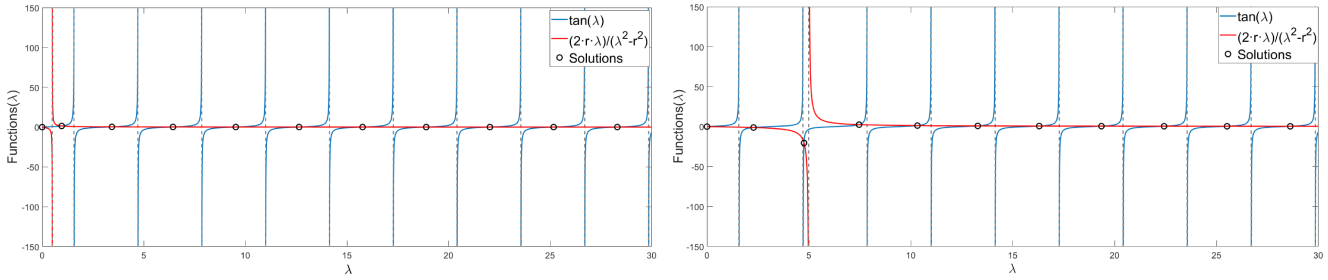

(A) Eigenvalues for $Pe = 1$ (B) Eigenvalues for $Pe = 10$

FIGURE 1 Representation of Equation (10) for $Pe = 1$ and $Pe = 10$. Its roots are the eigenvalues λ_n [Colour figure can be viewed at wileyonlinelibrary.com]

Due to $w(Z, \theta)$ has to verify the problem (8) and its boundary conditions, without taking into account the initial condition yet, the basic eigenfunctions are

$$X_n(Z) = \frac{\lambda_n}{r}\cos(\lambda_n Z) + \sin(\lambda_n Z), \tag{9}$$

where λ_n are the eigenvalues satisfying the equation

$$\tan(\lambda_n) = \frac{2\lambda_n r}{\lambda_n^2 - r^2}, \tag{10}$$

whose graph can be seen in Figure 1 for $Pe = 1$ and $Pe = 10$.

The equation satisfied by the eigenvalues is a transcendental equation, so a numerical method must be employed for its resolution. In Table 1, it can be seen a particular case of the values obtained after solving Equation (10).

3.2 | Resolution of the non-homogeneous heat equation

Using the *Fourier generalized development theorem*,[20] the solution of the equation

$$\frac{\partial w}{\partial \theta} = \frac{1}{2r}\frac{\partial^2 w}{\partial Z^2} + G(Z, \theta)$$

is of the form, in general,

$$w(Z, \theta) = \sum_{n=0}^{\infty} T_n(\theta) X_n(Z),$$

where $X_n(Z) = \frac{\lambda_n}{r}\cos(\lambda_n Z) + \sin(\lambda_n Z)$, whenever the eigenvalues λ_n verify Equation (10). The functions $T_n(\theta)$ have to satisfy the previous equation. The set formed by the proper functions $X_n(Z)$ and the mentioned λ_n constitutes an orthogonal basis. This property has been verified using `Matlab`. In our case, as $\lambda_0 = 0$:

$$w(Z, \theta) = \sum_{n=1}^{\infty} T_n(\theta) X_n(Z). \tag{11}$$

Assuming the suitable conditions of derivability and the convergence of the series given by the *Fourier generalized development theorem*, a relation that the functions $T_n(\theta)$ must verify can be obtained:

$$T_n'(\theta) + \frac{\lambda_n^2}{2r} T_n(\theta) = g_n(\theta), \forall n \geq 1.$$

where $g_n(\theta)$ are the Fourier coefficients of $G(Z, \theta)$ in the orthogonal basis $(X_n(Z))_{n=1}^{\infty}$.

It is worth noting two observations in order to facilitate the calculations. As it can be seen in the operations of the upper lines, the functions $G(Z,\theta)$ and $H(Z)$ are related, and therefore, their Fourier coefficients are in turn

$$G(Z,\theta) = se^{s\theta}[H(Z) - \varphi(Z)],$$

where the only term depending on the variable θ is the exponential factor. In general, $g_n(\theta) = se^{s\theta}(h_n - \varphi_n)$ being φ_n and h_n the Fourier coefficients of $\varphi(Z)$ and $H(Z)$, respectively,

$$h_n = \frac{1}{\int_0^1 X_n^2(Z)dZ}\int_0^1 H(Z)X_n(Z)dZ, \qquad \varphi_n = \frac{1}{\int_0^1 X_n^2(Z)dZ}\int_0^1 \varphi(Z)X_n(Z)dZ.$$

Summarizing, the functions $T_n(\theta)$ satisfy the IVP

$$\left.\begin{array}{ll} T_n'(\theta) + \frac{\lambda_n^2}{2r}T_n(\theta) & = se^{s\theta}(h_n - \varphi_n),\ \forall n \geq 1 \\ T_n(0) & = h_n \end{array}\right\}. \tag{12}$$

The solution of (12) is

$$T_n(\theta) = \frac{2rs(h_n - \varphi_n)}{2rs + \lambda_n^2}e^{s\theta} + \frac{2rs\varphi_n + h_n\lambda_n^2}{2rs + \lambda_n^2}e^{-\frac{\lambda_n^2}{2r}\theta}. \tag{13}$$

Finally, replacing (13) in (11) and undoing the changes of variable indicated in (3) and (6), the solution of the problem (2) is built by

$$C_{An}(Z,\theta) = e^{rZ - s\theta}\left(v(Z,\theta) + \sum_{n=1}^{\infty} T_n(\theta)X_n(Z)\right). \tag{14}$$

3.3 | Observations on the analytical solution

The convergence of all these functional series has been studied in the literature depending on the values of *Pe*. It can be demonstrated, applying the *M-Weierstrass criterion* in one case, or using *Comparison criterion* in another, that all the series involved are absolutely convergent and therefore convergent.[21,22] Golz and Dorroh[1] demonstrated that this series is bounded for all θ.

Besides, in this work, we considered for simulations the maximum dimensionless time, θ_{max}, which is shown in Table 2. It has been selected depending on the values of *Péclet* and *Damköhler* numbers, with the aim of reaching the steady state in the solution.

It can be observed that, for a fixed value of *Da*, the dimensionless time for achieving the steady state, θ_{max}, decreases when *Pe* increases. And this time also decreases for a fixed *Pe* when *Da* increases.

Throughout this paper, several considerations must be taken into account. In figures of the dimensionless concentration, for $C_{A0} = 0\,\text{mol/m}^3$ and $C_{Ae} = 1\,\text{mol/m}^3$, the picture on the left side shows the concentration profile: The time is fixed, and the position is variable. Only three values of θ have been chosen for clarity. θ_1 is the initial time, $\theta = 0$; the last value, θ_{10}, is when the system achieves approximately the steady state, that is, θ_{max}. Besides, an intermediate value, for example, $\theta_3 = \frac{2}{9}\theta_{max}$, has been assigned. On the other hand, the picture on the right side shows the evolution of the dimensionless concentration along the time for a fixed position in the reactor. Three Z positions are plotted: $Z = 0$, also denoted as node 1, $Z = 0.5$ approximately, indicated as middle node, and $Z = 1$, labeled as node $N + 1$.

This reference to nodes is not really necessary when an analytical solution is deduced, because it can be calculated at any Z position. Nevertheless, these plots will be compared in the following sections with those obtained using numerical methods based on a discretization scheme, where each Z position is associated to a node. This fact justifies the legends

TABLE 2 Value of θ_{max} from which the steady state is attained

Pe \ *Da*	**0.01**	**0.1**	**1**	**10**	**100**
0.01	8	7	4	1	0.1
0.1	8	7	4	1	0.1
1	8	7	4	1	0.1
10	5	4	3	1	0.05

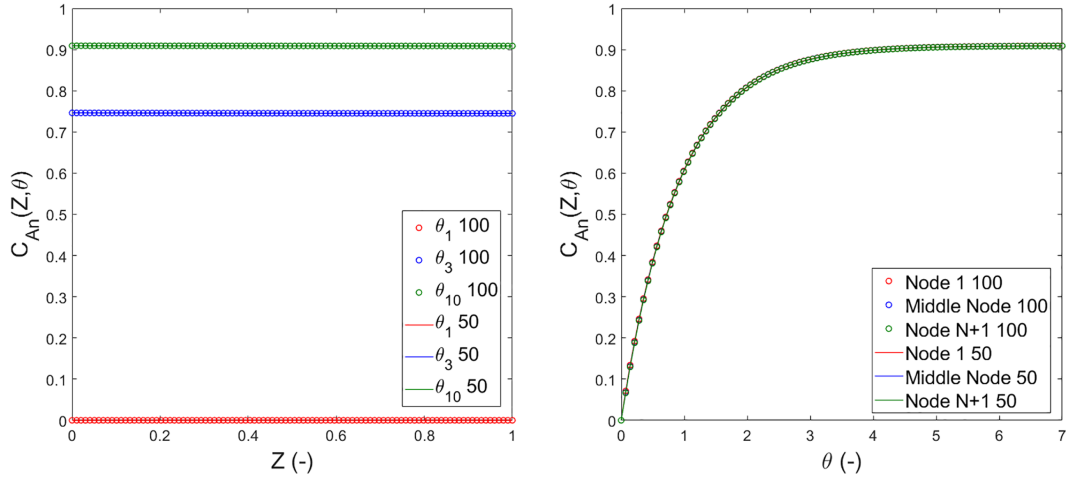

FIGURE 2 Representation of C_{An} obtained by the analytical technique for $Pe = 0.01$ and $Da = 0.1$ with 50 and 100 terms in Fourier expansion [Colour figure can be viewed at wileyonlinelibrary.com]

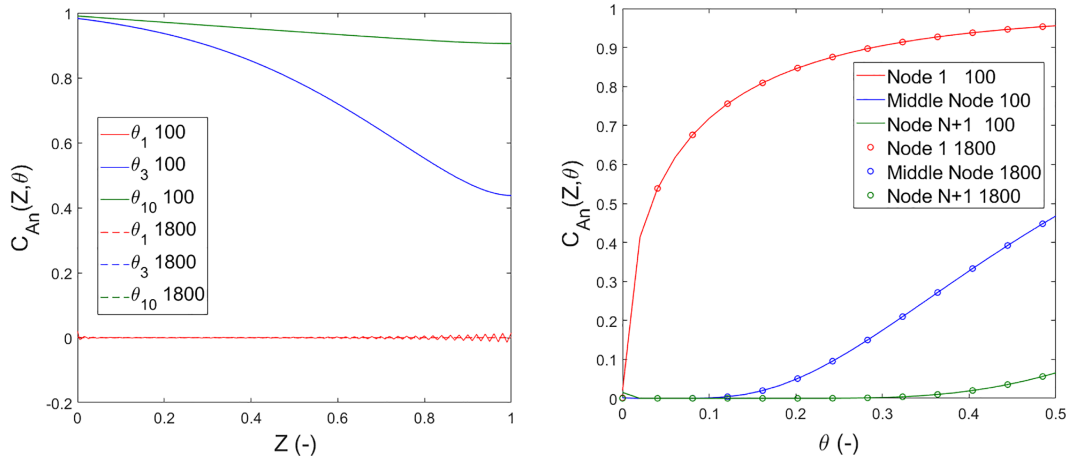

FIGURE 3 C_{An} curves for $Pe = 10$ and $Da = 0.1$ considering 100 and 1800 terms in the Fourier expansion in the analytical solution [Colour figure can be viewed at wileyonlinelibrary.com]

shown in the analytical plots. Although N can be any positive integer value, for the analytical solution obtained in this paper, $N = 100$ has been considered (101 nodes). Besides, a partition of 100 terms has been taken for $\theta \in [0, \theta_{max}]$.

It is important to realize that the analytical solution, (14), is a series. The first question to consider is the suitable number of n terms for calculation. Observe that for $Pe = 0.01$ and $Da = 0.1$ in Figure 2, there are no great variations in the obtained solution when the terms are increased from 50 to 100.

However, in Figure 3, where $Pe = 10$ and $Da = 0.1$, it can be seen in the picture on the left side that only at the initial time, θ_1, and near the reactor outlet ($Z = 1$) there are some small oscillations when merely 100 terms are considered. The same discrepancy can be observed in the picture on the right side, at the initial times and at the reactor outlet (node $N+1$). These perturbations disappear when the number of terms in the Fourier expansion is increased; see the same figure for 1800 terms.

Other dimensionless concentration curves for $Pe = 10$ and $Da = 100$ can be observed in Figure 4, where the same options in the number of terms of the Fourier development have been taken. A better observation of the improvement when 1800 terms are considered is shown in Figure 5.

Therefore, perturbations are found in the analytical solution when the number of terms is not suitable, depending on the particular values of Pe and Da. So the optimum number of terms has to be determined for avoiding these perturbations, without increasing unnecessarily the computation time.

For a specific value of Pe and Da, let $A_M \in \mathcal{M}_{100\times101}(\mathbb{R})$ be the matrix of the values of the dimensionless analytical concentration for (Z, θ) where M terms in the Generalized Fourier development are considered. Let us define TOL_M in

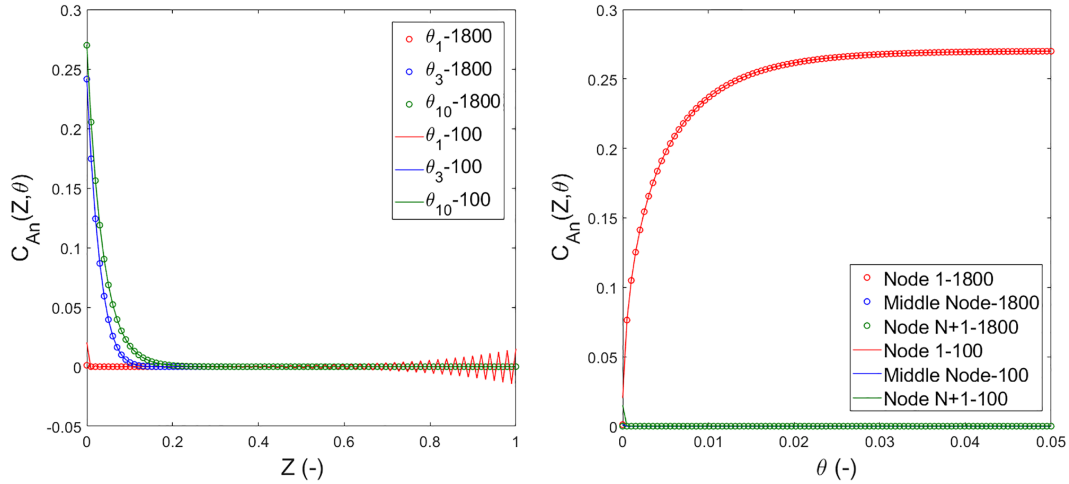

FIGURE 4 C_{An} curves for $Pe = 10$ and $Da = 100$ considering 100 terms and 1800 in the Fourier expansion in the analytical solution [Colour figure can be viewed at wileyonlinelibrary.com]

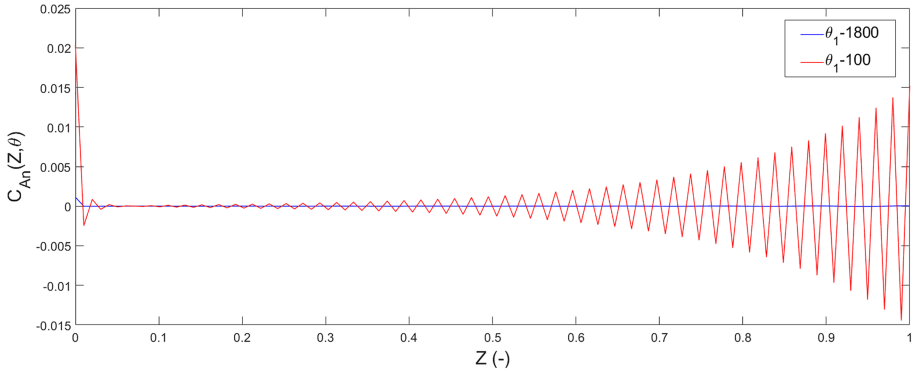

FIGURE 5 Detail in C_{An} curves for $Pe = 10$ and $Da = 100$ considering 100 terms or 1800 in the Fourier expansion for the analytical solution [Colour figure can be viewed at wileyonlinelibrary.com]

the following way:

$$TOL_M = \max_j(\max_i(|A_M - A_{M-100}|)). \tag{15}$$

TOL_M is a metric that measures how the precision of $C_{An}(Z,\theta)$ improves as the number of terms in the Fourier development increases. The question is which is the minimum number of terms M satisfying $TOL_M < 10^{-4}$, for each combination of Pe and Da values.

It can be seen in Figure 6 and in Table 3 that for a fixed *Péclet* number and several values of Da, the number of terms to consider is the same, regarding the tolerance defined by (15). This seems to indicate that *Damköhler* number has no influence in the number of terms to consider in Fourier development. This fact is owing to its contribution in the analytical expression of the considered differences in (15). Substituting (7) and (13) in (14), it is obtained

$$C_{An}(Z,\theta) = e^{rZ}\left[\frac{2}{2+r}(1+r-rZ) + \sum_{n=1}^{\infty} X_n(Z)\frac{2rs(h_n-\varphi_n) + (h_n\lambda_n^2 + 2rs\varphi_n)e^{-\left(s+\frac{\lambda_n^2}{2r}\right)\theta}}{2rs+\lambda_n^2}\right].$$

Calling C_{An}^M the partial sum with M terms in (14),

$$C_{An}^{M_2}(Z,\theta) - C_{An}^{M_1}(Z,\theta) = e^{rZ}\sum_{n=M_1+1}^{M_2}\frac{2rs(h_n-\varphi_n) + (h_n\lambda_n^2 + 2rs\varphi_n)e^{-\left(s+\frac{\lambda_n^2}{2r}\right)\theta}}{2rs+\lambda_n^2}X_n(Z)$$

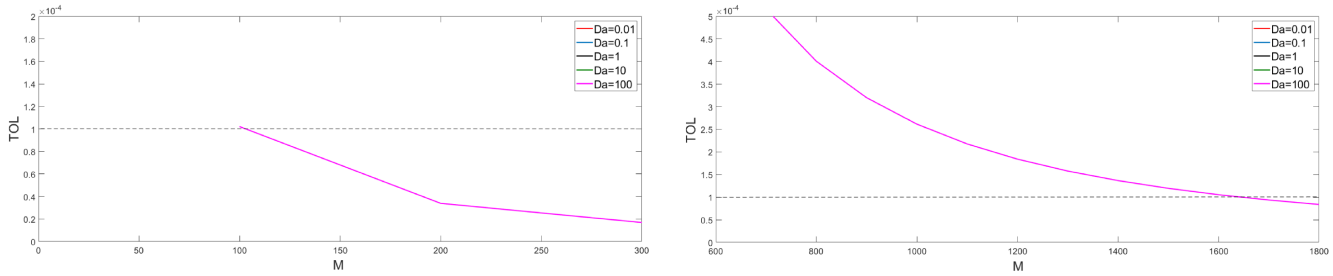

(A) $Pe = 0.1$ (B) $Pe = 10$

FIGURE 6 Number of terms in Fourier development for $Pe = 0.1$ and $Pe = 10$ with difference values of Da [Colour figure can be viewed at wileyonlinelibrary.com]

TABLE 3 Minimum number of terms in the Fourier Development for $TOL_M \leq 10^{-4}$

Pe \ Da	**0.01**	**0.1**	**1**	**10**	**100**
0.01	200	200	200	200	200
0.1	300	300	300	300	300
1	600	600	600	600	600
10	1800	1800	1800	1800	1800

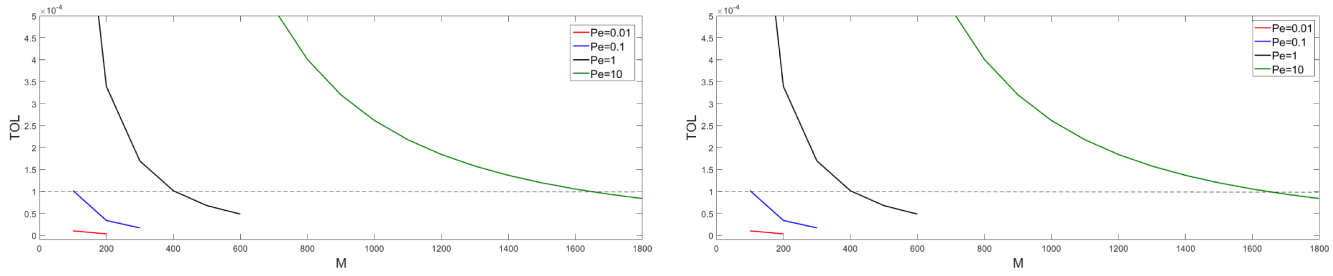

(A) $Da = 0.01$ (B) $Da = 10$

FIGURE 7 Number of terms in Fourier development for different values of Pe with $Da = 0.01$ and $Da = 10$ [Colour figure can be viewed at wileyonlinelibrary.com]

In the example described in this work, $\varphi_n = 0$ since $C_{A0} = 0$, then

$$C_{An}^{M_2}(Z,\theta) - C_{An}^{M_1}(Z,\theta) = e^{rZ} \sum_{n=M_1+1}^{M_2} h_n X_n(Z) \frac{2rs + \lambda_n^2 e^{-\left(s+\frac{\lambda_n^2}{2r}\right)\theta}}{2rs + \lambda_n^2}. \tag{16}$$

Obviously, when the number of terms to consider increases the sequence, $(\lambda_n)_n$ increases too; see Table 1. And so, since $s = \frac{Pe}{4} + Da$, the factor where Da is present decreases quickly to zero due to the exponential function incorporated in it.

However, if now Da is fixed and Pe is variable, a study about the number of the suitable terms to consider is shown in Figure 7.

If the value of Pe is increased the number of terms in the Fourier development also increases independently of the values of Da. All of this is summarized in Table 3.

It is worth noting that in Figure 2, no difference can be appreciated between the analytical solution when 100 terms against 50 terms are considered in the series development, for $Pe = 0.01$ and $Da = 0.1$. In Table 3, for those values of Pe and Da, 200 terms have been assigned. Figure 8 proves that it is not necessary to consider greater values of the number of terms. However, the data found using the formula (15) in the above table are due to the implemented algorithm. It has been applied starting from 100 terms, since in general for the other values of Pe at least this number of addends was necessary. In fact, $\max_j(\max_i(|A_{100} - A_{50}|)) = 2.0571 \cdot 10^{-5}$ is obtained. So the analytical solution for $Pe = 0.01$ could be

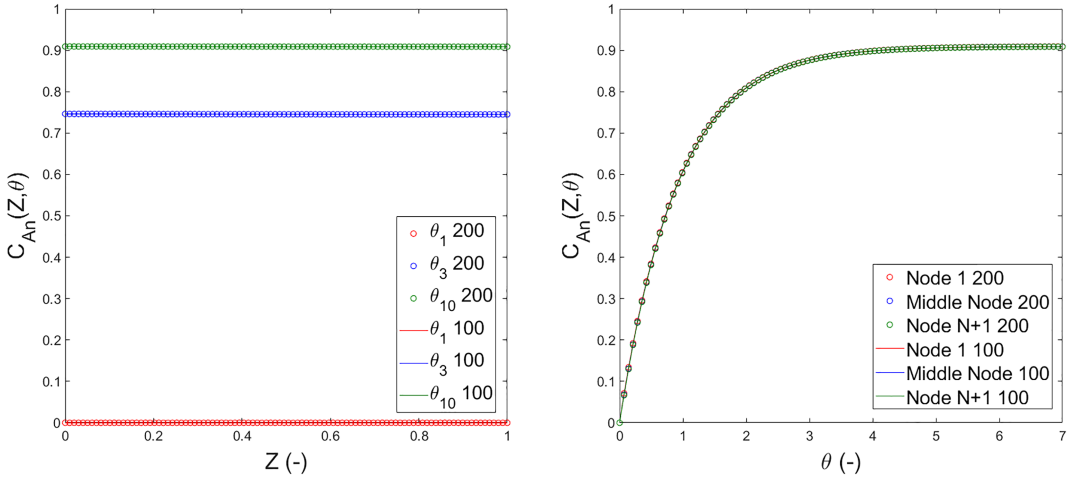

FIGURE 8 C_{An} curves for $Pe = 0.01$ and $Da = 0.1$ considering 100 and 200 terms in the Fourier expansion in the analytical solution [Colour figure can be viewed at wileyonlinelibrary.com]

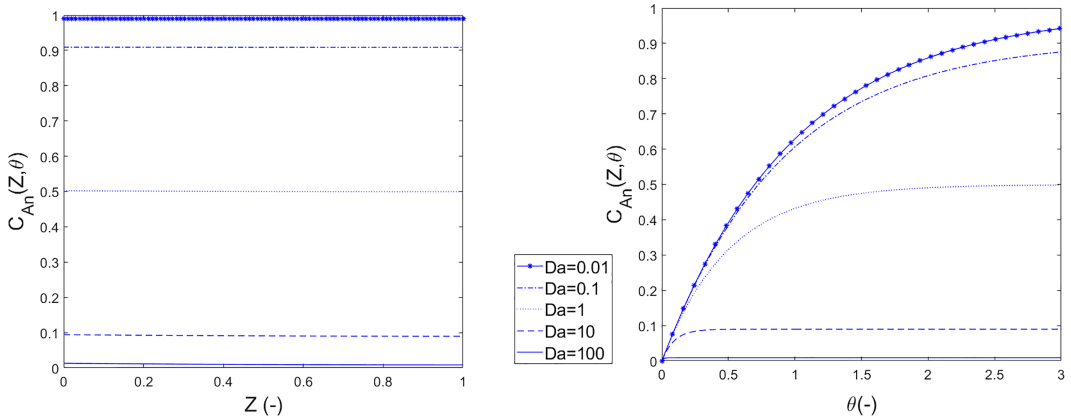

FIGURE 9 Representation of C_{An} in θ_{max} (left picture) and in node $N + 1$ (right picture) by analytical resolution with $Pe = 0.01$ and different values of Da [Colour figure can be viewed at wileyonlinelibrary.com]

calculated with 100 terms and the value of TOL_M of (15) is reached. Throughout this paper all the analytical solutions have been calculated with the optimum numbers of terms in the Fourier developments referred in Table 3.

Moreover, the data found in Table 3 lead us to the conclusion that for values of $Pe > 10$, the time of execution in `Matlab` would be so excessive. For this reason, these Pe values are not considered in this paper. On the other hand, those higher values of *Péclet* number in the convection–diffusion–reaction equation imply that diffusion is negligible versus convection and that the reactor behaves as a plug flow one. In this case, maybe it is better to solve directly the PDE corresponding to a plug flow reactor.

The dimensionless concentrations obtained by analytical resolution for a fixed value of *Péclet* and all the possible *Damköhler* numbers can be seen in Figures 9–11.

In Figure 9 $Pe = 0.01$, the right picture shows clearly that the steady state at the reactor outlet is reached earlier when the value of Da increases. The concentration curves are ever smooth and convex. And the values of the dimensionless concentration decrease as the value of Da becomes greater. This behavior also occurs along the reactor, not only at the outlet, as can be seen in the left picture.

In the previous figures, for $Pe = 1$ and $Pe = 10$, respectively, the concentration curves present an inflection point characteristic of the S-shaped curves. The change from concave to convex is more pronounced if Pe is bigger. In Figure 11, it can be seen that concentration reaches the steady state earlier than with the other values of Pe shown in Figures 9 and 10, right picture. For all these values of Pe, if greater values of Da are taken, this stationary aspect is reached at the initial stages. This observation can also be detected if the comparison study is done for a fixed Da together with all the possible *Péclet* numbers. In the right pictures of Figures 12 and 13, the outlet reactor concentration for some values of Da is shown.

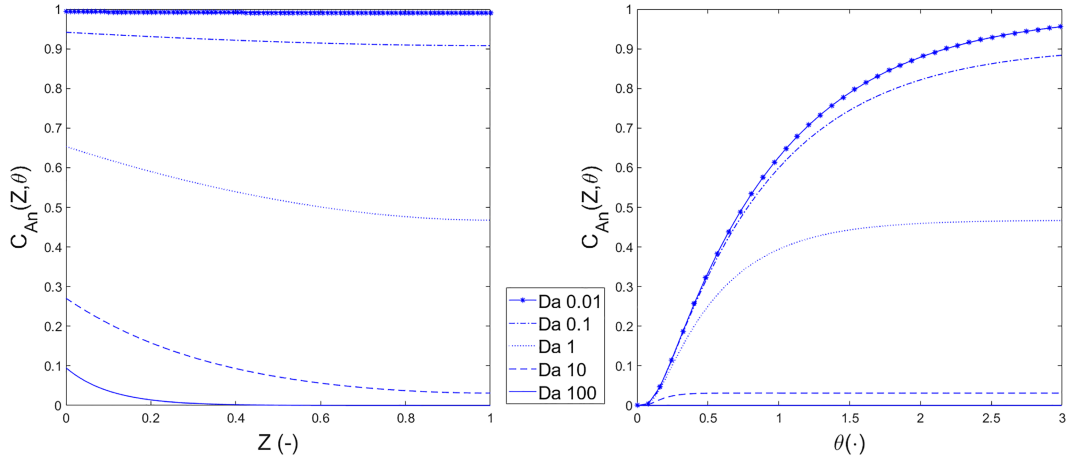

FIGURE 10 Representation of C_{An} in θ_{max} (left picture) and in node $N+1$ (right picture) by analytical resolution with $Pe = 1$ and different values of Da [Colour figure can be viewed at wileyonlinelibrary.com]

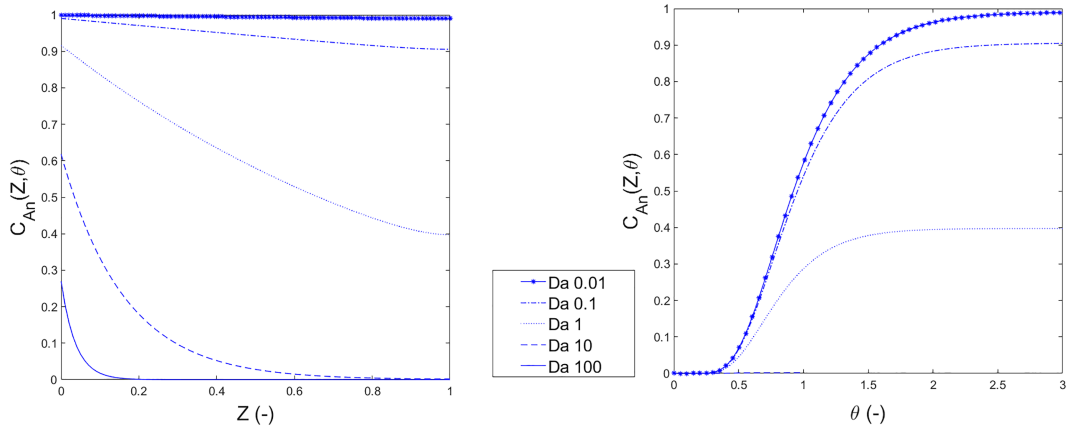

FIGURE 11 Representation of C_{An} in θ_{max} (left picture) and in node $N+1$ (right picture) by analytical resolution with $Pe = 10$ and different values of Da [Colour figure can be viewed at wileyonlinelibrary.com]

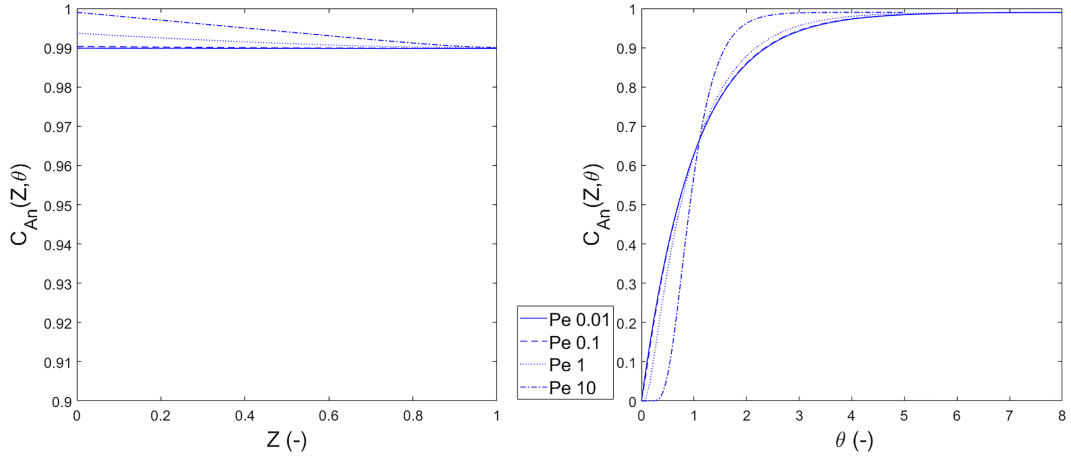

FIGURE 12 Representation of C_{An} in θ_{max} (left picture) and in node $N+1$ (right picture) by analytical resolution with $Da = 0.01$ and different values of Pe [Colour figure can be viewed at wileyonlinelibrary.com]

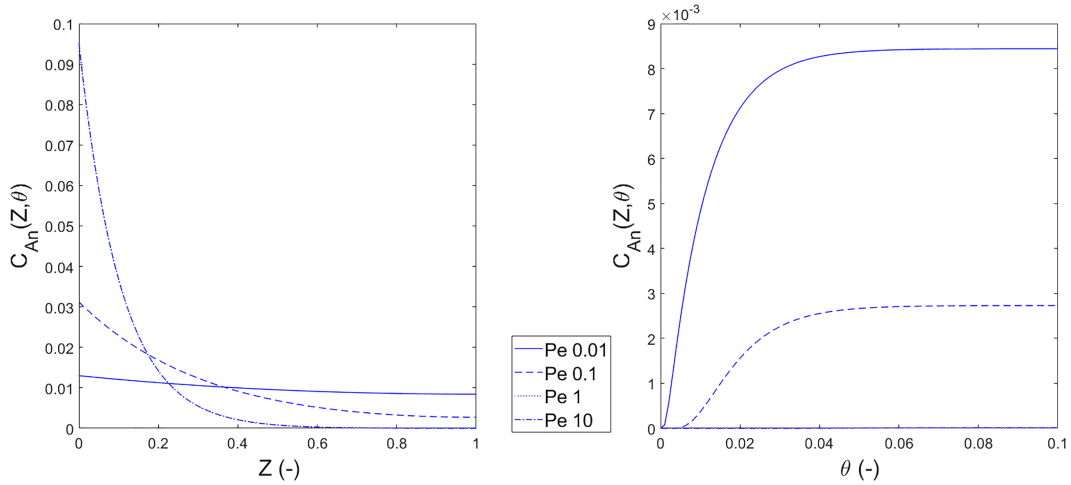

FIGURE 13 Representation of C_{An} in θ_{max} (left picture) and in node $N+1$ (right picture) by analytical resolution with $Da = 100$ and different values of Pe [Colour figure can be viewed at wileyonlinelibrary.com]

In the same way, clearly, for greater values of Da, the concentration curve at the reactor outlet reaches the stationary behavior earlier than for small values of Da. Note, moreover, the low values of the concentration as Pe increases.

4 | NUMERICAL RESULTS

Throughout this section, the normalized problem described in (2) is considered. To this problem, different numerical methods are applied to compare the results. Concretely, firstly, a unique discretization in spatial variable is done applying the MOL, and secondly, by using Crank–Nicholson, two discretizations, in spatial and time variables, are taken into account.

In the numerical methods that are described here, an internal mesh of equidistant partitions in each one of the domains is considered. Thus, for the spatial domain, with $Z \in [0,1]$, it is taken $Z_j = Z_0 + (j-1)h = (j-1)h$, where $j = 1, \dots, N+1$, $h = 1/N$; and for the time domain, $\theta \in [0,\infty)$, $\theta_n = \theta_0 + nk = nk, n = 0, \dots, M$ are considered where $k = \frac{\theta_{max}}{M}$ and θ_{max} is shown in Table 2.

We denote

$$\begin{aligned} C_j &= C_{An}(Z_j,\theta),\ j = 1, \dots, N+1 \\ C_j^n &= C_{An}(Z_j,\theta_n),\ j = 1, \dots, N+1, n = 0, \dots, M, \end{aligned}$$

for MOL and Crank–Nicholson, respectively.

Usually, only internal points are taken in the mesh, $j = 2, \dots, N$ and $n = 1, \dots, M-1$. Depending on the boundary conditions for the problem, there exist different possibilities to work with those points.

4.1 | Strategies for the boundary conditions

In the case of Dirichlet boundary conditions, after the spatial discretization, the variables associated to both endpoints of the spacial grid have directly assigned a numerical value. However, if Neumann or Robin boundary conditions are given and a method that discretizes derivatives with respect to the spatial variable is used, several ways can be followed.

For example, using a second-order central difference scheme,[13]

$$\begin{aligned} \left.\frac{\partial f}{\partial Z}\right|_{Z_j} &= \frac{f_{j+1}-f_{j-1}}{2\Delta Z} + O(\Delta Z^2), \\ \left.\frac{\partial^2 f}{\partial Z^2}\right|_{Z_j} &= \frac{f_{j+1}-2f_j+f_{j-1}}{\Delta Z^2} + O(\Delta Z^2), \end{aligned} \tag{17}$$

for the equation corresponding to the jth row of the system matrix, it would be necessary to know the previous and subsequent data. This would be a problem when working at the grid endpoints because there is no previous data for $Z = 0$ and there is no further data for $Z = 1$.

The solution is either to apply what is called "false frontier" or "fictitious nodes"[13] or in the grid endpoints to use a system of progressive differences in $Z = 0$ and regressive ones in $Z = 1$:

$$\begin{aligned} \left.\frac{\partial f}{\partial Z}\right|_{Z_1} &\simeq \frac{-3f_1+4f_2-f_3}{2\Delta Z} + O(\Delta Z^2) \text{ Forward Difference,} \\ \left.\frac{\partial f}{\partial Z}\right|_{Z_{N+1}} &\simeq \frac{3f_{N+1}-4f_N+f_{N-1}}{2\Delta Z} + O(\Delta Z^2) \text{ Backward Difference,} \end{aligned} \tag{18}$$

which is the strategy applied here. For this reason, the equations of both numerical methods, MOL and Crank-Nicholson's scheme, apply only for internal nodes of the mesh; that is, from $j = 2, \ldots, N$. Besides, concretely, the equations for $j = 2$ and for $j = N$ allow us to obtain the values of C_1 and C_{N+1} which are replacing in this internal grid.

4.2 | About the stability and consistency of the numerical methods

A method is called stable when the rounding or truncation errors generated in each of the iterations do not greatly affect the output data. Let be the local error of a numerical method at a point (Z_j, θ_n) like the committed error when applying the algorithm once at that point with the considered step in each of the independent variables. A method is said to be consistent of order p if p is the largest integer such that the maximum of the quotient between the local error and the step is an $O(h^p)$. The consistency of a method measures whether the solutions of the problem, when the step considered in the grid tends to zero, approximate the solutions of the discrete problem, supposing that the truncation error of the development of Taylor tends to zero.[23]

Thanks to the Lax theorem,[24] it is known that a consistent and stable method is convergent. There are several ways to study the stability of a numerical method applied to an ODE or algebraic problem, such as the Von Neumann's method and the spectral radius of the matrix method.[20] In this paper, both mentioned methods will be followed.

Let a numerical method described by an equation be like

$$C^{n+1} = MC^n + U^n.$$

Let C_e^n be the exact solution in the nth iteration of the method and e^n the truncation or rounding error produced in the nth iteration. With these notations, it can be written

$$C^n = C_e^n + e^n. \tag{19}$$

Both the exact solution and the numerical solution verify the equation where the discretization has already been applied. So subtracting the following expressions, you get

$$\left.\begin{array}{l} C_e^{n+1} = MC_e^n + U^n \\ C^{n+1} = MC^n + U^n \iff C_e^{n+1} + e^{n+1} = M(C_e^n + e^n) + U^n \end{array}\right\} \Rightarrow e^{n+1} = Me^n. \tag{20}$$

A necessary condition for having a stable method is

$$\lim_{n\to\infty} ||e^n|| = 0, \tag{21}$$

with some adequate vector norm, giving rise to conditions on the chosen steps in the temporal and spatial discretization.

Obviously, considering the matrix norm induced by the vector norm taking in (19), the sequence of errors given in (21) must be contractive. If the 1-norm matrix, also called spectral norm, is used, it is known that a necessary and sufficient condition for this purpose is[20]

$$\rho(M) = \max_k |\lambda_k| < 1,$$

being $\rho(M)$ the spectral radius of the matrix M obtained in (20) and being λ_k the eigenvalues of this matrix.[25]

On the other hand, in the Von Neumann's method for the study of the stability, a periodic solution of the equation is supposed admitting an expression of the form $C(Z, \theta) = T(\theta)e^{iPZ}$, where i is the imaginary unit and P is the period.[24] In

the case studied here, this requisite is verified as has been seen in previous sections. And then,

$$C_j^n = T^n e^{iPjh}.$$

So for the stability of the method, it must be verified that

$$\left|\frac{T^{n+1}}{T^n}\right| < 1. \tag{22}$$

This amplification quotient will be studied for Crank–Nicholson's method described in the following sections.

4.3 | MOL

To apply MOL to the problem (2), the cylindrical reactor is divided into N slices, which generates $N+1$ nodes. To each of these nodes, it is assigned the dimensionless time-dependent variable $C_j(\theta)$ with $j = 1, \ldots, N+1$, so that

$$C_j(\theta) = C_{An}\left(Z_j, \theta\right), j = 1, \ldots, N+1,$$

where

$$Z_j = \frac{j-1}{N}, j = 1, \ldots, N+1,$$

all this scheme can be seen in Figure 14.

MOL consists of transforming the PDE, with its initial and boundary conditions, into a system of ODEs with their corresponding initial conditions, discretizing only the spatial variable. For this purpose, partial spatial derivatives must be replaced by finite differences. In this case, since it is a parabolic PDE due to the diffusive term in Equation (2), finite

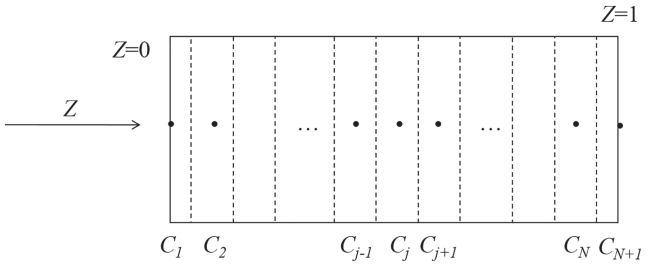

FIGURE 14 MOL scheme, $j = 1, \ldots, N+1$

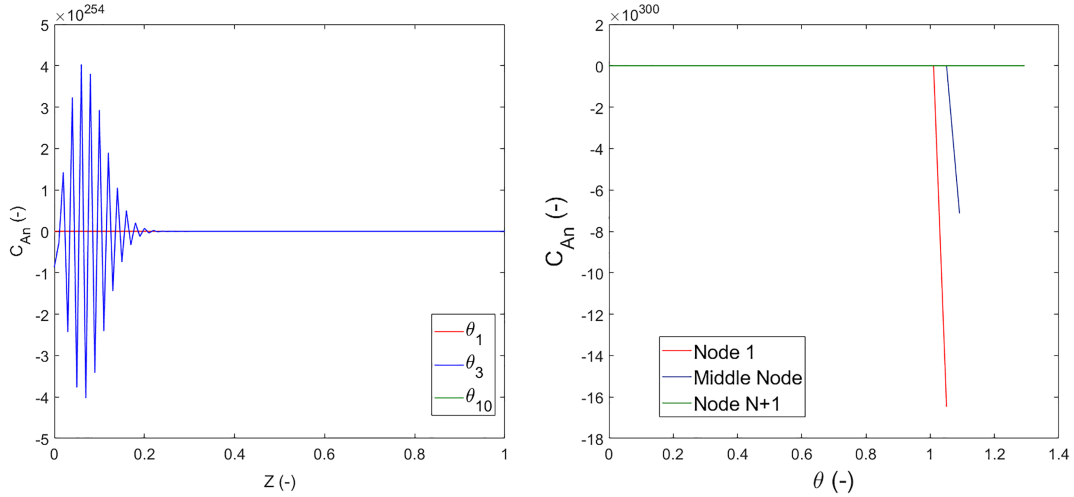

FIGURE 15 Representation of the concentration curves obtained for $Pe = 0.1$ and $Da = 1$ using MOL with the built-in Matlab fixed-step `ode3` solver, incorporated only in older `Matlab` versions and not distributed in modern ones ($N = 100$) [Colour figure can be viewed at wileyonlinelibrary.com]

TABLE 4 Values of $\Delta\theta$ against ΔZ_{stab} for several values of *Péclet* and *Damköhler* numbers

	Da									
	0.01		**0.1**		**1**		**10**		**100**	
Pe	$\Delta\theta$	ΔZ_{stab}	$\Delta\theta$	ΔZ_{stab}	$\Delta\theta$	ΔZ_{stab}	$\Delta\theta$	ΔZ_{stab}	$\Delta\theta$	ΔZ_{stab}
0.01	$8.1\cdot10^{-2}$	$5.0\cdot10^{-7}$	$7.1\cdot10^{-2}$	$5.0\cdot10^{-7}$	$4.0\cdot10^{-2}$	$5.0\cdot10^{-7}$	$1.0\cdot10^{-2}$	$5.0\cdot10^{-7}$	$1.0\cdot10^{-3}$	$5.0\cdot10^{-7}$
0.1	$8.1\cdot10^{-2}$	$5.0\cdot10^{-6}$	$7.1\cdot10^{-2}$	$5.0\cdot10^{-6}$	$4.0\cdot10^{-2}$	$5.0\cdot10^{-6}$	$1.0\cdot10^{-2}$	$5.0\cdot10^{-6}$	$1.0\cdot10^{-3}$	$5.0\cdot10^{-6}$
1	$8.1\cdot10^{-2}$	$5.0\cdot10^{-5}$	$7.1\cdot10^{-2}$	$5.0\cdot10^{-5}$	$4.0\cdot10^{-2}$	$5.0\cdot10^{-5}$	$1.0\cdot10^{-2}$	$5.0\cdot10^{-5}$	$1.0\cdot10^{-3}$	$5.0\cdot10^{-5}$
10	$5.1\cdot10^{-2}$	$4.8\cdot10^{-4}$	$4.0\cdot10^{-2}$	$4.8\cdot10^{-4}$	$3.0\cdot10^{-2}$	$4.8\cdot10^{-4}$	$1.0\cdot10^{-2}$	$4.8\cdot10^{-4}$	$5.1\cdot10^{-4}$	$4.7\cdot10^{-4}$

central second-order differences, (17), will be used at the internal grid points, while forward or backward second-order finite differences are used for Robin and Neumann boundary conditions, (18).

Let us begin with *B.C.*1, which allows obtain information from C_1. To do this, $\frac{\partial C_{An}}{\partial Z}\Big|_{Z=0}$ is replaced by the second-order forward finite difference approximation for the first derivative:

$$1 = C_1 - \frac{1}{Pe}\frac{-3C_1 + 4C_2 - C_3}{\frac{2}{N}}.$$

Operating, C_1 is obtained:

$$C_1 = \frac{2\frac{Pe}{N} + 4C_2 - C_3}{2\frac{Pe}{N} + 3}.$$

*B.C.*2 allows to determine C_{N+1}. Therefore, $\frac{\partial C_{An}}{\partial Z}\Big|_{Z=1}$ is replaced by the second-order backward finite difference approximation corresponding to the first derivative:

$$\frac{3C_{N+1} - 4C_N + C_{N-1}}{\frac{2}{N}} = 0.$$

Operating,

$$C_{N+1} = \frac{4C_N - C_{N-1}}{3}.$$

Finally, the discretization of the PDE allows to obtain information about C_j , with $j = 2, \dots, N$. For this, the PDE is applied in each of the nodes $j = 2, \dots, N$, and $\frac{\partial C_{An}}{\partial Z}$ is replaced in Z_j by the second-order central finite difference for the first derivative, while $\frac{\partial^2 C_{An}}{\partial Z^2}$ in Z_j is replaced by the second-order central finite difference for the second derivative, obtaining the following system of $N-1$ ODEs:

$$\frac{dC_j}{d\theta} = -\frac{C_{j+1} - C_{j-1}}{\frac{2}{N}} + \frac{1}{Pe}\frac{C_{j+1} - 2C_j + C_{j+1}}{\left(\frac{1}{N}\right)^2} - Da\cdot C_j,\ j = 2, \dots, N, \tag{23}$$

with the following initial conditions:

$$C_j(0) = \frac{C_{A0}}{C_{Ae}},\ j = 2, \dots, N.$$

4.3.1 | Stability of the MOL for the convection–diffusion–reaction equation

In the assumption that the solution of the problem (2) is periodic in the studied domain, several works have been found in the literature,[20] which states that the method is stable if the following relationship between the discretization time step, $\Delta\theta = k$, and the discretization spatial step, $\Delta Z = h$, is verified:

$$\Delta\theta \le \Delta Z_{stab} := \frac{1}{\frac{1}{\Delta Z} + \frac{2}{Pe\Delta Z^2} + \frac{Da}{2}}. \tag{24}$$

When working with `Matlab` to solve the obtained system of ODEs, the user can find several built-in variable-step numerical methods, combinations of different Runge–Kutta, and other numerical routines for the ODEs resolution. If

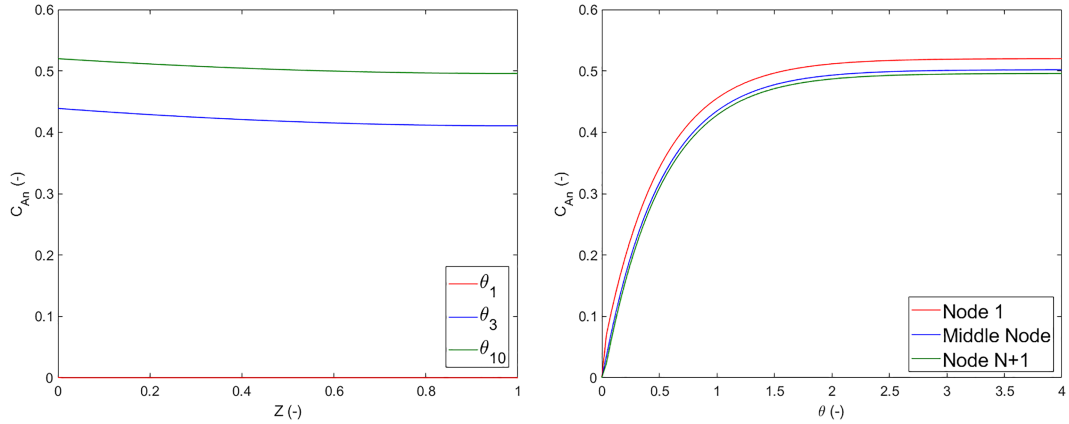

FIGURE 16 Representation of the concentration curves obtained for $Pe = 0.1$ and $Da = 1$ using MOL with the built-in Matlab variable-step `ode15s` solver ($N = 100$) [Colour figure can be viewed at wileyonlinelibrary.com]

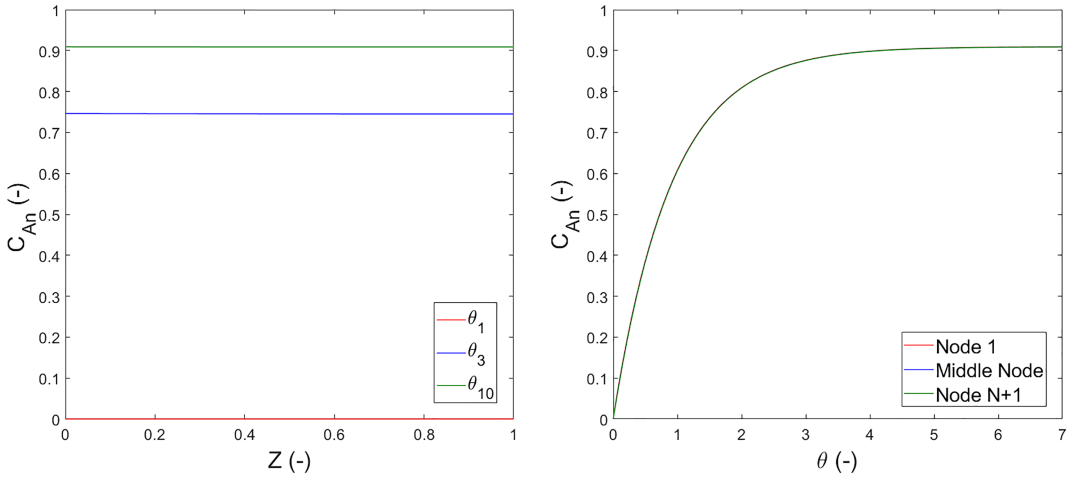

FIGURE 17 Representation of the concentration curves obtained for $Pe = 0.01$ and $Da = 0.1$ using MOL with the built-in Matlab variable-step `ode15s` solver ($N = 100$) [Colour figure can be viewed at wileyonlinelibrary.com]

other fixed-step routines are used, the solutions are not always stable (Figure 15). This non-stable behavior is expected taking into account Table 4, where $\Delta\theta$ applied in each simulation is compared to the quotient (24), using $\Delta Z = 0.01$. For all the combinations of *Pe* and *Da* values used in this paper, relation (24) is not fulfilled.

In order to get stable solutions, according to Equation (24), smaller discretization time-step values should be used, which is not efficient when executing the implemented programs. For this reason, this paper has worked with `Matlab` built-in variable-step ODE solvers, concretely, the `ode15s` solver. The values of the obtained concentration can be observed in Figure 16 for the same *Péclet* and *Damköhler* values taken in Figure 15.

The solutions obtained with the variable-step `ode15s` solver are stable. Other ODEs solvers can be used in `Matlab`, but the results are not considerably better. Other example of solutions found with MOL are seen in Figures 17–19 taking $N = 100$.

4.4 | Crank–Nicholson's method

This method applies discretization to both time and spatial derivatives, this being one of its main differences with the MOL that only discretizes the spatial derivatives. With this discretization MOL leads to a system of ordinary differential equations, while Crank–Nicholson solves a system of algebraic equations.

On the other hand, the Crank–Nicholson's method achieves greater stability than MOL since it is based on working with the numerical approximation to the value of the solution of the convection–diffusion–reaction equation in a middle node of the mesh of the type $(Z, \theta + k/2)$; see Figure 20. It is an implicit method, which can lead to greater operational complexity, but a stable method is obtained,[26] for all $\frac{k}{h^2}$.[27]

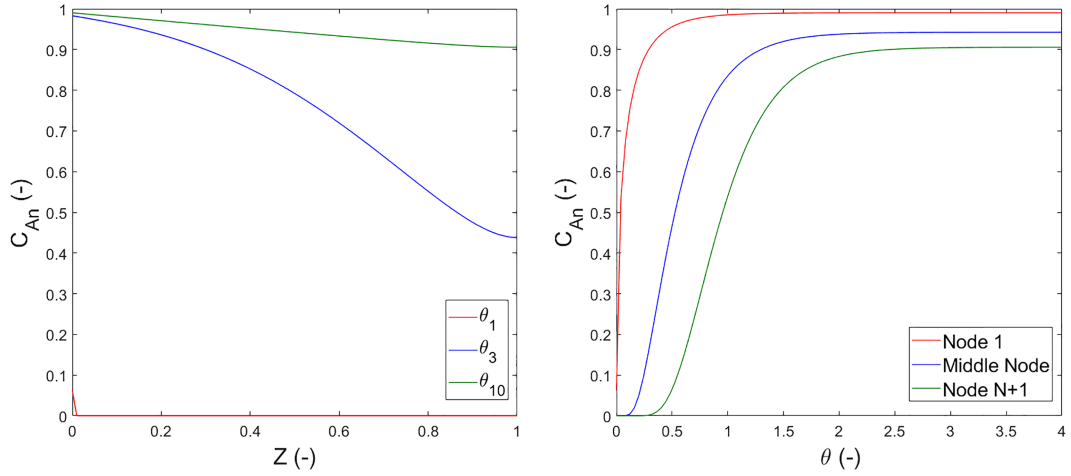

FIGURE 18 Representation of the concentration curves obtained for $Pe = 10$ and $Da = 0.1$ using MOL with the built-in Matlab variable-step `ode15s` solver ($N = 100$) [Colour figure can be viewed at wileyonlinelibrary.com]

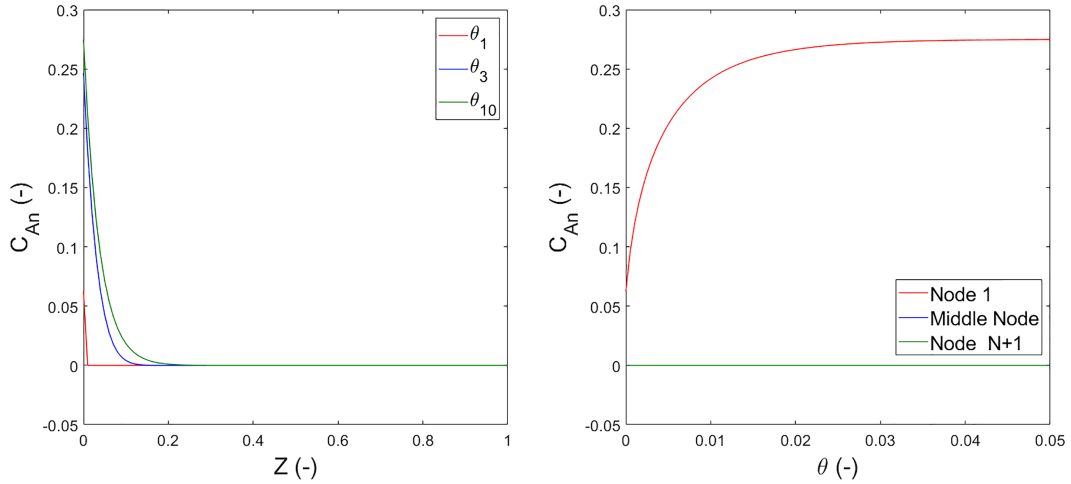

FIGURE 19 Representation of the concentration curves obtained for $Pe = 10$ and $Da = 100$ using MOL with the built-in Matlab variable-step `ode15s` solver ($N = 100$) [Colour figure can be viewed at wileyonlinelibrary.com]

FIGURE 20 Grid of Crank–Nicholson's method, $j = 1, \ldots, N+1$, $n = 0, \ldots, M$

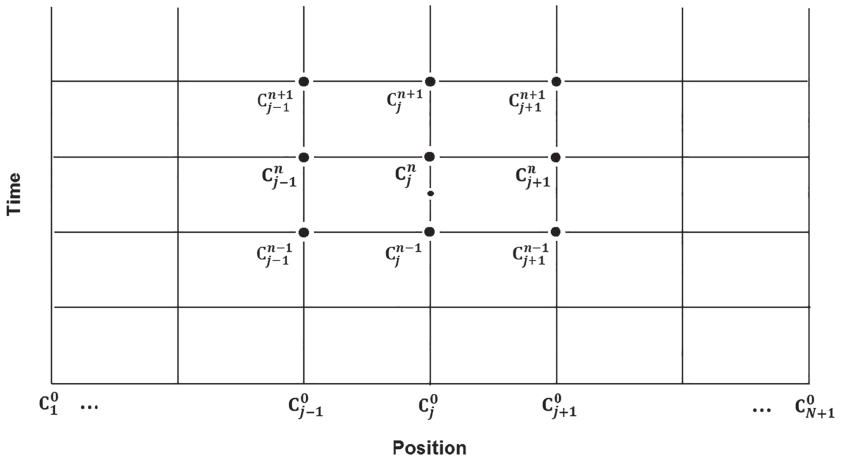

For the time derivative, the second-order central difference scheme for the first derivative seen in (17) is directly applied, using $\Delta\theta = k/2$:

$$\frac{\partial C_{An}}{\partial \theta}(Z, \theta + k/2) = \frac{C_{An}(Z, \theta + k) - C_{An}(Z, \theta)}{k} + O(k^2).$$

While for the second-order spatial derivatives, the average of the central differences obtained for the expressions of $\frac{\partial^2 C_{An}}{\partial Z^2}(Z,\theta+k)$ and $\frac{\partial^2 C_{An}}{\partial Z^2}(Z,\theta)$ is done, applying the formulas of (17). Analogously for the spatial derivatives of first order, the mean value of the second-order central differences applied to $\frac{\partial C_{An}}{\partial Z}(Z,\theta+k)$ and $\frac{\partial C_{An}}{\partial Z}(Z,\theta)$ is again taken. The following approximations or equations of the method are obtained[28]:

$$C_{An} = \frac{C_j^{n+1} + C_j^n}{2} + O(k^2),$$

$$\frac{\partial C_{An}}{\partial Z} = \frac{C_{j+1}^{n+1} - C_{j-1}^{n+1} + C_{j+1}^n - C_{j-1}^n}{4h} + O(h^2),$$

$$\frac{\partial^2 C_{An}}{\partial Z^2} = \frac{C_{j+1}^{n+1} - 2C_j^{n+1} + C_{j-1}^{n+1} + C_{j+1}^n - 2C_j^n + C_{j-1}^n}{2h^2} + O(h^2).$$

Therefore, remembering that the dimensionless PDE that models the problem is

$$\frac{\partial C_{An}}{\partial \theta} = -\frac{\partial C_{An}}{\partial Z} + \frac{1}{Pe}\frac{\partial^2 C_{An}}{\partial Z^2} - DaC_{An},$$

it is obtained for $j = 2, \ldots, N$, $n = 0, \ldots, M-1$:

$$\frac{C_j^{n+1} - C_j^n}{k} = -\left(\frac{C_{j+1}^{n+1} - C_{j-1}^{n+1} + C_{j+1}^n - C_{j-1}^n}{4h}\right) + \frac{1}{Pe}\left(\frac{C_{j+1}^{n+1} - 2C_j^{n+1} + C_{j-1}^{n+1} + C_{j+1}^n - 2C_j^n + C_{j-1}^n}{2h^2}\right) - Da\left(\frac{C_j^{n+1} + C_j^n}{2}\right).$$

To propose the matrices of the method, the values of iteration $n+1$ should be moved to the left-hand side of the equation and the iteration n to the right-hand one. First, the equations that verify the internal nodes of the mesh are considered, that is, $j = 2, \ldots, N$:

$$\begin{aligned} C_{j+1}^{n+1}\left(\tfrac{1}{4h} - \tfrac{1}{2h^2Pe}\right) + C_j^{n+1}\left(\tfrac{1}{k} + \tfrac{1}{h^2Pe} + \tfrac{Da}{2}\right) + C_{j-1}^{n+1}\left(\tfrac{-1}{4h} - \tfrac{1}{2h^2Pe}\right) \\ = C_{j+1}^{n}\left(\tfrac{-1}{4h} + \tfrac{1}{2h^2Pe}\right) + C_j^{n}\left(\tfrac{1}{k} - \tfrac{1}{h^2Pe} - \tfrac{Da}{2}\right) + C_{j-1}^{n}\left(\tfrac{1}{4h} + \tfrac{1}{2h^2Pe}\right), \end{aligned} \tag{25}$$

noting that this matrix formulation gives rise to tridiagonal matrices.

For the study of the boundary conditions, we work with progressive differences in the case of $Z = 0$ and with regressive differences in the case of $Z = 1$. Specifically we use non-centered differences with three points, (18).[20] Given $n = 0, \ldots, M$:

$$\begin{aligned} \left.\frac{\partial C_{An}}{\partial Z}\right|_{Z=0} &= \frac{-3C_1^n + 4C_2^n - C_3^n}{2h} \overset{B.C.1}{=} -Pe + PeC_1^n \Rightarrow C_1^n = \frac{2hPe + 4C_2^n - C_3^n}{3 + 2hPe}, \\ \left.\frac{\partial C_{An}}{\partial Z}\right|_{Z=1} &= \frac{3C_{N+1}^n - 4C_N^n + C_{N-1}^n}{2h} \overset{B.C.2}{=} 0 \Rightarrow C_{N+1}^n = \frac{4C_N^n - C_{N-1}^n}{3}. \end{aligned} \tag{26}$$

Replacing these values in the equations of the method for $j = 2$,

$$\begin{aligned} C_2^{n+1}\left[\frac{1}{k} + \frac{1 + hPe}{h^2Pe(3 + 2hPe)} + \frac{Da}{2}\right] + C_3^{n+1}\left[\frac{h^2Pe^2 - 2}{2h^2Pe(3 + 2hPe)}\right] \\ = C_2^n\left[\frac{1}{k} - \frac{Da}{2} - \frac{1 + hPe}{h^2Pe(3 + 2hPe)}\right] + C_3^n\left[\frac{-h^2Pe^2 + 2}{2h^2Pe(3 + 2hPe)}\right] + \frac{2 + hPe}{h(3 + 2hPe)}, \end{aligned}$$

and then for $j = N$,

$$\begin{aligned} C_{N-1}^{n+1}\left[\frac{-1}{3h} - \frac{1}{3h^2Pe}\right] + C_N^{n+1}\left[\frac{1}{3h} + \frac{1}{k} + \frac{1}{3h^2Pe} + \frac{Da}{2}\right] \\ = C_{N-1}^n\left[\frac{1}{3h} + \frac{1}{3h^2Pe}\right] + C_N^n\left[\frac{1}{k} - \frac{Da}{2} - \frac{1}{3h} - \frac{1}{3h^2Pe}\right]. \end{aligned}$$

TABLE 5 Values of $k = \frac{\theta_{max}}{M}$ against $\frac{2}{Da}$ for several values of *Péclet* and *Damköhler* numbers and $M = 99$

		Da									
		0.01		**0.1**		**1**		**10**		**100**	
		k	$\frac{2}{Da}$	k	$\frac{2}{Da}$	k	$\frac{2}{Da}$	k	$\frac{2}{Da}$	k	$\frac{2}{Da}$
Pe	0.01	0.08	200	0.07	20	0.04	2	0.01	0.2	0.001	0.02
	0.1	0.08	200	0.07	20	0.04	2	0.01	0.2	0.001	0.02
	1	0.08	200	0.07	20	0.04	2	0.01	0.2	0.001	0.02
	10	0.05	200	0.04	20	0.03	2	0.01	0.2	0.0005	0.02

TABLE 6 Values of $k = \frac{\theta_{max}}{M}$ against $\frac{2}{Da}$ for several values of *Péclet* and *Damköhler* numbers and $M = 495$

		Da									
		0.01		**0.1**		**1**		**10**		**100**	
		k	$\frac{2}{Da}$	k	$\frac{2}{Da}$	k	$\frac{2}{Da}$	k	$\frac{2}{Da}$	k	$\frac{2}{Da}$
Pe	0.01	0.016	200	0.014	20	0.008	2	0.002	0.2	0.0002	0.02
	0.1	0.016	200	0.014	20	0.008	2	0.002	0.2	0.0002	0.02
	1	0.016	200	0.014	20	0.008	2	0.002	0.2	0.0002	0.02
	10	0.05	200	0.008	20	0.006	2	0.002	0.2	0.0001	0.02

It is possible to reformulate the numerical method by means of a system of equations for the internal grid. We have a system whose matrix $A \in \mathcal{M}_{N-1}(\mathbb{R}), B \in \mathcal{M}_{N-1}(\mathbb{R})$ and whose expression is

$$AC^{n+1} = BC^n + U^n,\ n = 0, 1, \dots, M-1, \tag{27}$$

being

$$A = \begin{pmatrix} \frac{1}{k} + \frac{1+hPe}{h^2Pe(3+2hPe)} + \frac{Da}{2} & \frac{h^2Pe^2-2}{2h^2Pe(3+2hPe)} & 0 & \dots & 0 \\ \frac{-1}{4h} - \frac{1}{2h^2Pe} & \frac{1}{k} + \frac{1}{h^2Pe} + \frac{Da}{2} & \frac{1}{4h} - \frac{1}{2h^2Pe} & 0 & \dots & 0 \\ \ddots & \ddots & \ddots & & & \\ & & \frac{-1}{4h} - \frac{1}{2h^2Pe} & \frac{1}{k} + \frac{1}{h^2Pe} + \frac{Da}{2} & \frac{1}{4h} - \frac{1}{2h^2Pe} & \\ 0 & \dots & 0 & \frac{-1}{3h} - \frac{1}{3h^2Pe} & \frac{1}{3h} + \frac{1}{k} + \frac{1}{3h^2Pe} + \frac{Da}{2} \end{pmatrix},$$

with

$$C^n = \begin{pmatrix} C_2^n \\ \vdots \\ C_N^n \end{pmatrix},\ C^{n+1} = \begin{pmatrix} C_2^{n+1} \\ \vdots \\ C_N^{n+1} \end{pmatrix},\ U^n = \begin{pmatrix} \frac{2+hPe}{h(3+2hPe)} \\ 0 \\ \vdots \\ 0 \end{pmatrix},$$

and

$$B = \begin{pmatrix} \frac{1}{k} - \frac{Da}{2} - \frac{1+hPe}{h^2Pe(3+2hPe)} & \frac{-h^2Pe^2+2}{2h^2Pe(3+2hPe)} & 0 & \dots & 0 \\ \frac{1}{4h} + \frac{1}{2h^2Pe} & \frac{1}{k} - \frac{1}{h^2Pe} - \frac{Da}{2} & \frac{-1}{4h} + \frac{1}{2h^2Pe} & 0 & \dots & 0 \\ \ddots & \ddots & \ddots & & & \\ & & \frac{1}{4h} + \frac{1}{2h^2Pe} & \frac{1}{k} - \frac{1}{h^2Pe} - \frac{Da}{2} & \frac{-1}{4h} + \frac{1}{2h^2Pe} & \\ 0 & \dots & 0 & \frac{1}{3h} + \frac{1}{3h^2Pe} & \frac{1}{k} - \frac{Da}{2} - \frac{1}{3h} - \frac{1}{3h^2Pe} \end{pmatrix}.$$

Note that the initial condition of the problem (2) ensures that $C_{An}(Z, 0) = \frac{C_{A0}}{C_{Ae}} = C_j^0, \forall j = 1, \dots, N+1$. It is suffices consider a spatial step $h < \frac{\sqrt{2}}{Pe}$, which is easily achievable for the *Pe* and *Da* values and for the partition spatial here considered; and a temporal step $k < \frac{2}{Da}$, which, as you will see in Tables 5 and 6, is always verified in this work. Taking into account all these assumptions, the matrix A is a strictly diagonally dominant, and so it is invertible assuring the existence of unique solution of the algebraic system.

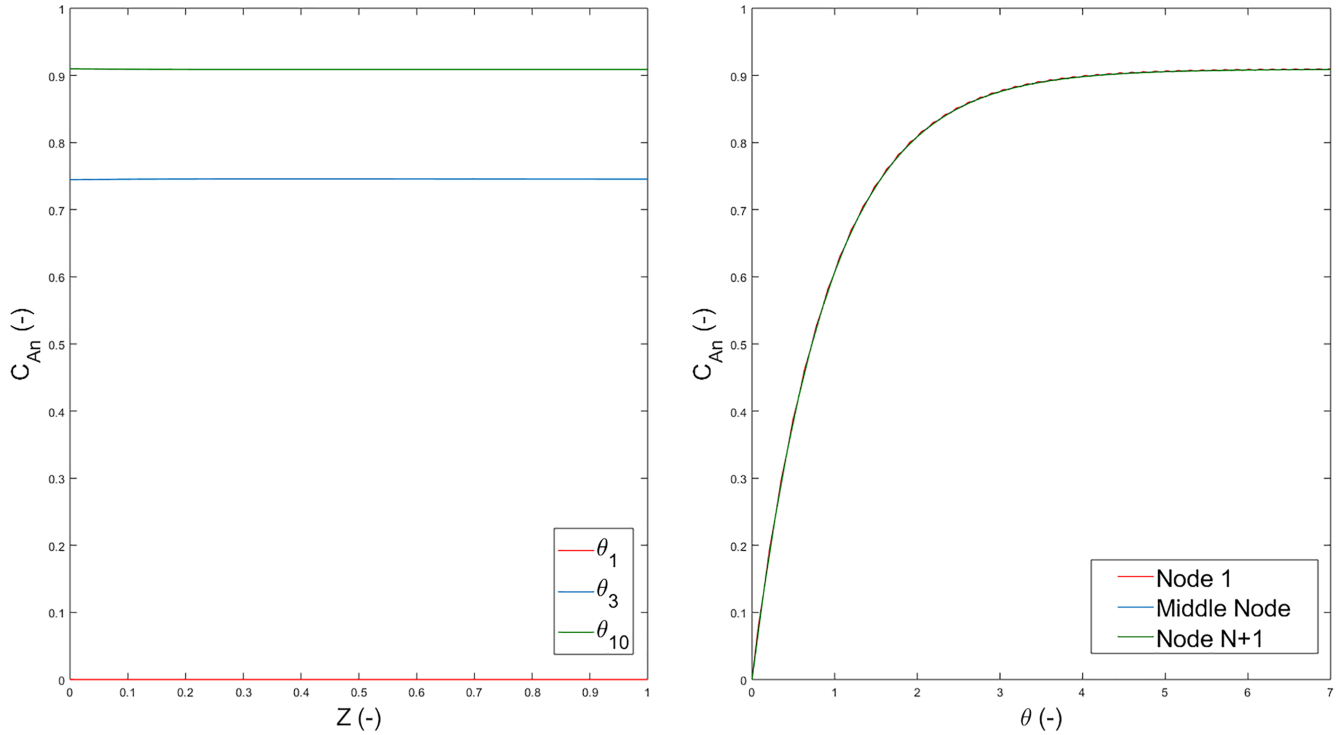

FIGURE 21 Representation of the concentration curves obtained for $Pe = 0.01$ and $Da = 0.1$ using Crank–Nicholson's method with $N = 100, M = 99$ [Colour figure can be viewed at wileyonlinelibrary.com]

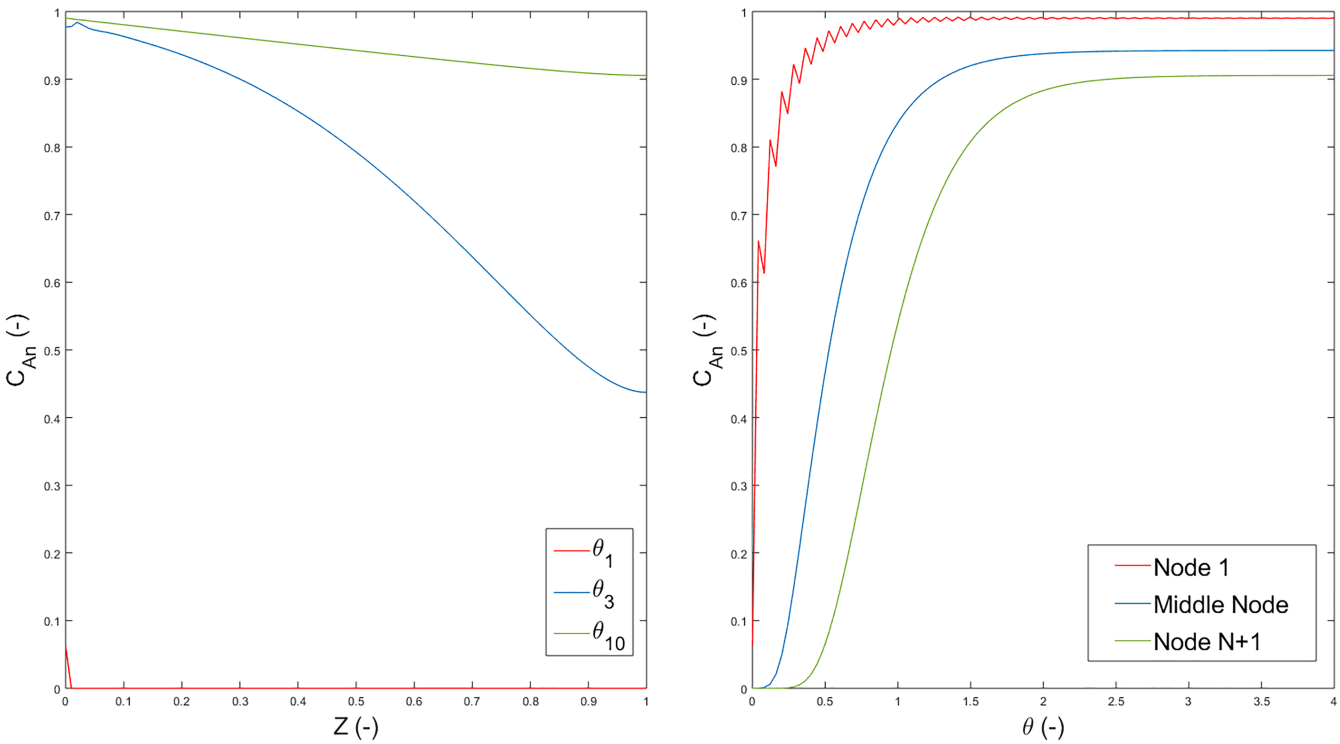

FIGURE 22 Representation of the concentration curves obtained for $Pe = 10$ and $Da = 0.1$ using Crank–Nicholson's method with $N = 100, M = 99$ [Colour figure can be viewed at wileyonlinelibrary.com]

When the system solution has already been obtained by a direct method, the values of C_1^n and C_{N+1}^n, $n = 0, \ldots, M$ are calculated taking into account the expressions given in (26). Numerical results for $N = 100, M = 99$ can be seen in Figures 21–23 for the same values of *Péclet* and *Damköhler* numbers illustrated in the previous methods.

It can be observed, for example, in Figure 22, that in the first nodes, Crank–Nicholson's method presents worse results than MOL, Figure 18. However, this disadvantage is overcame taking a finer temporary partition in Crank–Nicholson's method, for example ,$M = 495$. That is, only it is necessary to increase the number of iterations. An example of this improvement is illustrated in Figure 24.

Although in some cases it is not necessary to make $M = 495$ iterations in Crank–Nicholson's method, as is illustrated in Figures 21 and 23, Table 7 indicates for which values of Pe and Da is more suitable to take into account $M = 495$. It can be seen that considering $Da = 10^n$, if $n < 1$, the oscillations increase for bigger values of Pe; conversely, taking $n \geq 1$ these oscillations in the first spatial nodes decrease as Pe increases. So throughout this paper, all the Crank–Nicholson solutions have been calculated with $M = 495$.

4.4.1 | Stability and convergence of the Crank–Nicholson's method for the convection–diffusion–reaction equation with Danckwerts conditions

The consistency of the Crank–Nicholson's method applied to the convection–diffusion equation can be seen in Zuazua[24] and Carranza.[29] In the case studied here, a reaction term has been added to the PDE. It can be verified that this does not influence the time consistency of the method. Therefore, by the Lax theorem, it would suffice to study the stability of the Crank–Nicholson's method for the problem equation (2). In the Crank–Nicholson's method, it is discretized both in time and space; then, this condition must necessarily be verified.

If the technique of the spectral radius were analytically used for the study of stability,[25] eigenvalues of complicated calculations would be obtained for large values of N. However, a study for the different values of Pe and Da here taken are performed. The matrix of method (27) is $A^{-1}B$, so the following table is obtained for all these values.

Table 8 shows that the matrix of Crank–Nicholson's method for the values of Pe and Da here considered has, in general, all the eigenvalues strictly less than the unit, although very close to that value. Even so, it can be concluded from this that the Crank–Nicholson's method with Danckwerts conditions is stable for the problem (2) since the spectral radius of the matrix of the method $\rho(A^{-1}B) < 1$. These values so close to one make us think of taking concrete temporal steps and spatial steps. When the heat equation is studied, it is customary to take $\Delta\theta = Pe(\Delta Z)^2$.[24] It is a future line of research not taken into account here since the main purpose in this paper is trying to study the methods under the same spacing conditions in the mesh.

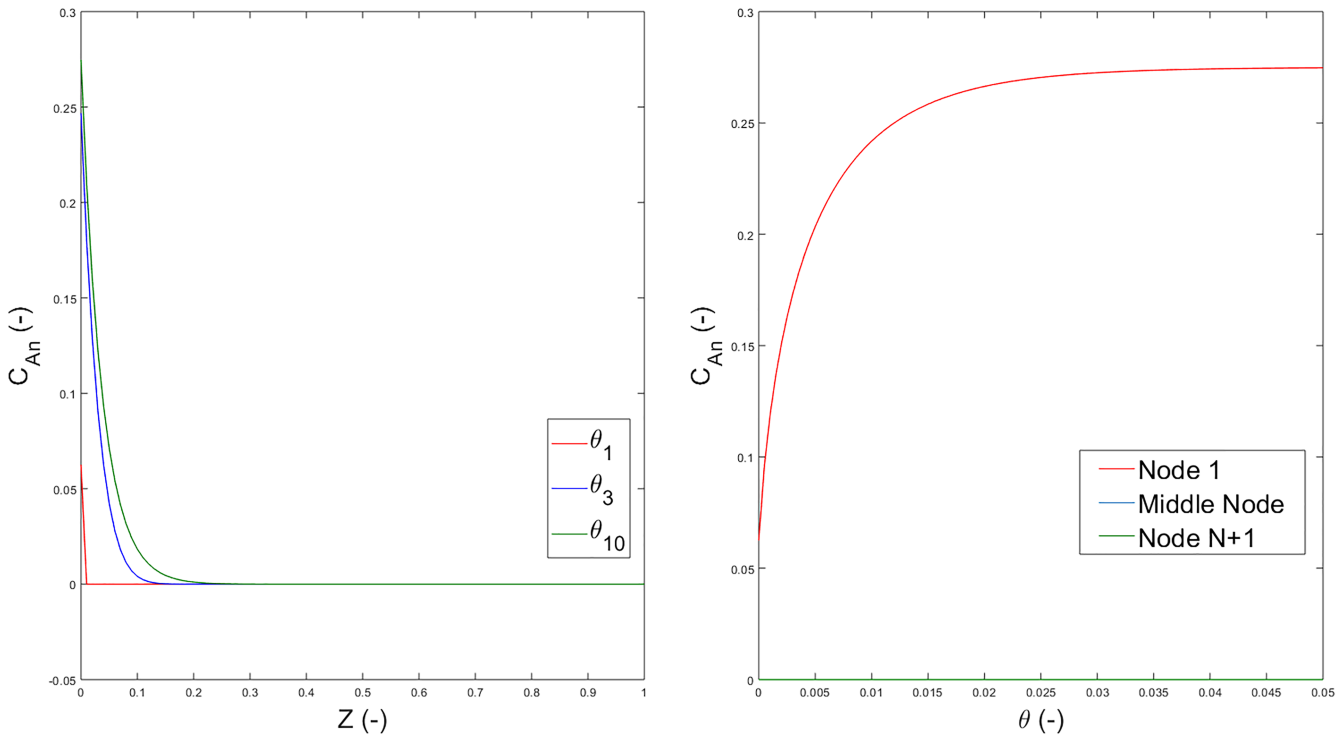

FIGURE 23 Representation of the concentration curves obtained for $Pe = 10$ and $Da = 100$ using Crank–Nicholson's method with $N = 100, M = 99$ [Colour figure can be viewed at wileyonlinelibrary.com]

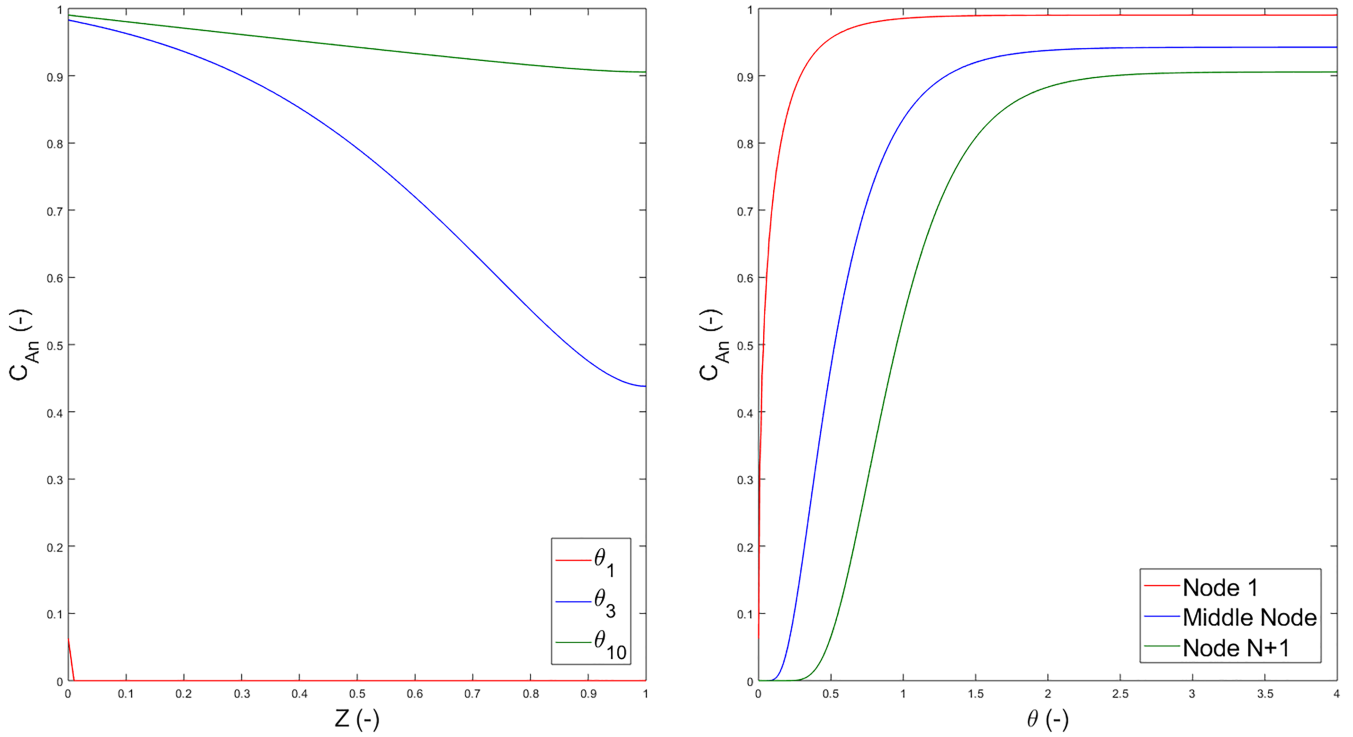

FIGURE 24 Representation of the concentration curves obtained for $Pe = 10$ and $Da = 0.1$ using Crank–Nicholson's method with $N = 100$ and $M = 495$ [Colour figure can be viewed at wileyonlinelibrary.com]

Noteworthy, that another way to demonstrate the stability of the method of the previous problem would be using the Von Neumann method, see (22). We start, as it is already known, with the calculation of the analytic periodic solution expressed as

$$C_j^n = T^n e^{iPjh},$$

where P is the period of the solution.

Replacing this in the equation of the method seen in (25), internal grid, the modulus of the amplification quotient $\frac{T^{n+1}}{T^n}$ is given by

$$\left|\frac{T^{n+1}}{T^n}\right|^2 = \frac{\left[1 - \frac{kDa}{2} - \frac{k}{h^2Pe} + \frac{k}{h^2Pe}\cos(Ph)\right]^2 + \frac{k}{4h^2}\sin^2(Ph)}{\left[1 + \frac{k}{h^2Pe} - \frac{k}{h^2Pe}\cos(Ph) + \frac{kDa}{2}\right]^2 + \frac{k}{4h^2}\sin^2(Ph)}.$$

Calling $\alpha = \frac{k}{h^2Pe}$,

$$\left|\frac{T^{n+1}}{T^n}\right|^2 = \frac{\left[1 - \frac{kDa}{2} - \alpha(1 - \cos(Ph))\right]^2 + \frac{\alpha Pe}{4}\sin^2(Ph)}{\left[1 + \frac{kDa}{2} + \alpha(1 - \cos(Ph))\right]^2 + \frac{\alpha Pe}{4}\sin^2(Ph)}. \tag{28}$$

To demonstrate that the condition of the Von Neumann's method is satisfied, (22), it is enough to observe that it is always true

$$2\alpha(1 - \cos(Ph)) \geq 0.$$

Firstly, if $1-\cos(Ph) = 0$ is obvious to check that $\sin(Ph) = 0$ and so, $\left|\frac{T^{n+1}}{T^n}\right| < 1$ since $kDa > 0$. Due to this fact, from now on, let $2\alpha(1-\cos(Ph)) > 0$. Taking into account the product $2[kDa+2\alpha(1-\cos(Ph))]$ where each one of the factors corresponds

TABLE 7 Number of iterations M in Crank–Nicholson's method

Pe \ Da	**0.01**	**0.1**	**1**	**10**	**100**
0.01	99	99	99	495	495
0.1	495	495	495	495	495
1	495	495	495	495	99
10	495	495	495	495	99

TABLE 8 Minimum and maximum, respectively, of the eigenvalues of $A^{-1}B$ in Crank–Nicholson's method

Pe \ Da	**0.01**	**0.1**	**1**	**10**	**100**
0.01	$[-0.99, 0.98]$	$[-0.99, 0.98]$	$[-0.99, 0.98]$	$[-0.99, 0.97]$	$[-0.99, 0.98]$
0.1	$[-0.99, 0.98]$	$[-0.99, 0.98]$	$[-0.99, 0.98]$	$[-0.99, 0.97]$	$[-0.95, 9.80]$
1	$[-0.99, 0.98]$	$[-0.99, 0.98]$	$[-0.98, 0.98]$	$[-0.95, 0.97]$	$[-0.60, 0.97]$
10	$[-0.90, 0.97]$	$[-0.88, 0.97]$	$[-0.84, 0.97]$	$[-0.60, 0.97]$	$[0.65, 0.99]$

TABLE 9 Rate of convergence of CN method with Danckwerts conditions for $Da = 0.01$

θ_n \ Pe	**0.01**	**0.1**	**1**	**10**
θ_1	0.9999	0.9993	0.9928	0.9307
θ_{25}	1.0336	1.1080	1.3116	1.8906
θ_{50}	1.0480	1.1547	1.3889	1.9640
θ_{75}	1.0588	1.1883	1.4349	1.9282
θ_{100}	1.0683	1.2158	1.4755	1.9105

to the sum and the difference, respectively, of the terms which appear squared in the amplification quotient (28)

$$
\begin{aligned}
0 &< 2\left[kDa + 2\alpha(1-\cos(Ph))\right] \\
&= \left[1+\left(\frac{kDa}{2}+\alpha(1-\cos(Ph))\right)\right]^2 - \left[1-\left(\frac{kDa}{2}+\alpha(1-\cos(Ph))\right)\right]^2 \\
&= \left[1+\left(\frac{kDa}{2}+\alpha(1-\cos(Ph))\right)\right]^2 + \frac{\alpha Pe}{4}\sin^2(Ph) - \left[1-\left(\frac{kDa}{2}+\alpha(1-\cos(Ph))\right)\right]^2 - \frac{\alpha Pe}{4}\sin^2(Ph) \\
&= \left[1+\left(\frac{kDa}{2}+\alpha(1-\cos(Ph))\right)\right]^2 + \frac{\alpha Pe}{4}\sin^2(Ph) - \left[\left[1-\left(\frac{kDa}{2}+\alpha(1-\cos(Ph))\right)\right]^2 + \frac{\alpha Pe}{4}\sin^2(Ph)\right]
\end{aligned}
$$

or equivalently,

$$
\left[1+\left(\frac{kDa}{2}+\alpha(1-\cos(Ph))\right)\right]^2 + \frac{\alpha Pe}{4}\sin^2(Ph) > \left[1-\left(\frac{kDa}{2}+\alpha(1-\cos(Ph))\right)\right]^2 + \frac{\alpha Pe}{4}\sin^2(Ph).
$$

This fact leads to conclude that

$$
\left|\frac{T^{n+1}}{T^n}\right|^2 < 1 \iff \left|\frac{T^{n+1}}{T^n}\right| < 1.
$$

Analogously, the process can be developed for the equations of the boundary nodes, (26).

With one of these proofs the stability is demonstrated, which together with the consistency gives the convergence of the method using Lax theorem.

Besides convergence, other important concept when a numerical method is worked is the rate of convergence. The rate of convergence of Crank–Nicholson's method with Danckwerts conditions has been studied using the definition seen in Jeong et al.[30] Firstly, let be denoted by $C^n_{i,\Delta Z_h} \approx C(Z_i, \theta_n)$ with $\Delta Z_h := (\Delta Z)_h = 1/h$. Taking into account this notation, let be define the error in the hth iteration by

$$
\varepsilon^n_{i,h} = \left|C^n_{i,(\Delta Z)_h} - C^n_{i,(\Delta Z)_{h-1}}\right|,
$$

θ_n \ Pe	**0.01**	**0.1**	**1**	**10**
θ_1	0.9999	0.9993	0.9928	0.9307
θ_{25}	1.0469	1.1521	1.3886	1.9412
θ_{50}	1.0664	1.2111	1.4740	1.9166
θ_{75}	1.0837	1.2567	1.5831	1.9229
θ_{100}	1.0955	1.2836	1.7208	1.9223

TABLE 10 Rate of convergence of CN method with Danckwerts conditions for $Da = 1$

θ_n \ Pe	**0.01**	**0.1**	**1**	**10**
θ_1	0.9999	0.9993	0.9928	0.9307
θ_{25}	1.3013	1.8904	1.9544	1.8915
θ_{50}	1.3681	1.9800	1.9541	1.8859
θ_{75}	1.4872	1.9829	1.9541	1.8846
θ_{100}	1.5424	1.9836	1.9541	1.8843

TABLE 11 Rate of convergence of CN method with Danckwerts conditions for $Da = 100$

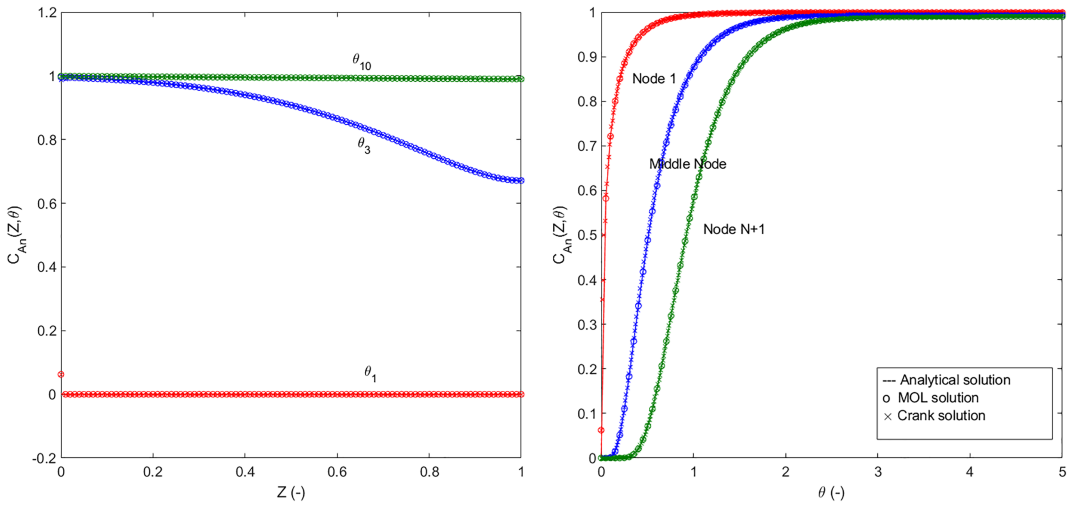

FIGURE 25 Different representations of the concentration C_{An} with $Pe = 10$ and $Da = 0.01$ using the three methods for the resolution [Colour figure can be viewed at wileyonlinelibrary.com]

and so, the vector $\varepsilon_{N_Z}^{N_\theta} = (\varepsilon_1^{N_\theta}, \varepsilon_2^{N_\theta} \ \dots \ , \varepsilon_{N_Z}^{N_\theta})$ is obtained; let

$$||\varepsilon_{N_Z}^{N_\theta}||_2 := \sqrt{\frac{\sum_{i=1}^{N_Z} (\varepsilon_{i,h}^{N_\theta})^2}{N_Z}}.$$

All the possible cases of values of Pe and Da have been studied, but only any results are shown in Tables 9–11, considering $M = 495{,}990$ and the $N = 100{,}200{,}400$:

The previous tables shown that the CN method for the problem (2) has a rate of convergence of order two, approximately, in a wide variety of cases but there are some values of Pe and Da for which linear convergence radius is obtained. Besides, it can be seen that the radius of convergence increases when Da increases, generally unless $Da = 100$ and $Pe = 10$.

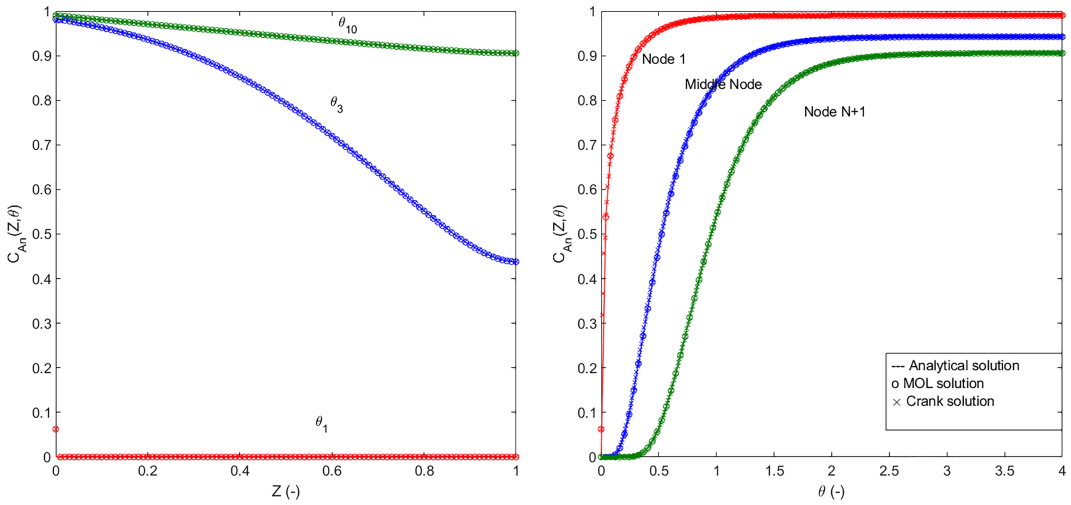

FIGURE 26 Different representations of the concentration C_{An} with $Pe = 10$ and $Da = 0.1$ using the three methods for the resolution [Colour figure can be viewed at wileyonlinelibrary.com]

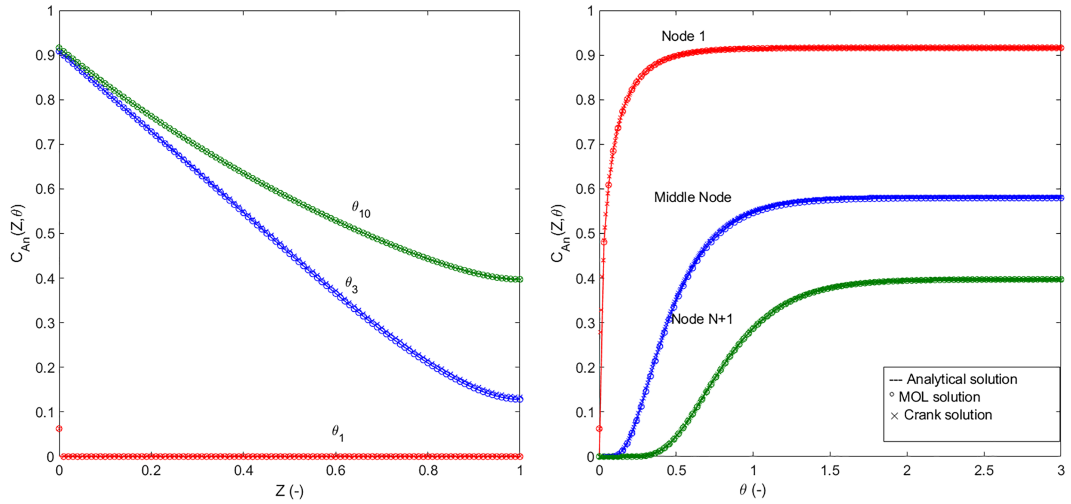

FIGURE 27 Different representations of the concentration C_{An} with $Pe = 10$ and $Da = 1$ using the three methods for the resolution [Colour figure can be viewed at wileyonlinelibrary.com]

TABLE 12 Maximum error, ϵ_{max}, between analytical and MOL matrix solutions with $N = 100$ and its associated position

Pe \ Da	**0.01**	**0.1**	**1**	**10**	**100**
0.01	$1.00 \cdot 10^{-4}$ [0, 1]	$1.00 \cdot 10^{-4}$ [0, 1]	$1.00 \cdot 10^{-4}$ [0, 1]	$2.68 \cdot 10^{-2}$ [0, 1]	$1.80 \cdot 10^{-2}$ [48, 1]
0.1	$6.00 \cdot 10^{-4}$ [0, 1]	$6.00 \cdot 10^{-4}$ [0, 1]	$6.00 \cdot 10^{-4}$ [0, 1]	$4.60 \cdot 10^{-4}$ [0, 1]	$4.60 \cdot 10^{-4}$ [0, 1]
1	$6.30 \cdot 10^{-3}$ [0, 1]	$6.30 \cdot 10^{-3}$ [0, 1]	$6.30 \cdot 10^{-3}$ [0, 1]	$6.30 \cdot 10^{-3}$ [0, 1]	$6.30 \cdot 10^{-3}$ [0, 1]
10	$6.14 \cdot 10^{-2}$ [0, 1]	$6.14 \cdot 10^{-2}$ [0, 1]	$6.14 \cdot 10^{-2}$ [0, 1]	$6.14 \cdot 10^{-2}$ [0, 1]	$6.14 \cdot 10^{-2}$ [0, 1]

5 | COMPARATIVE STUDY

In this section, we present a comparison among the different solutions found by the three methods studied here. The analysis has been done in a mathematical and a graphical way. First of all, the graphics obtained with each one of the applied methods have been represented in the same axis, as an example for $Pe = 10$ and $Da \in \{0.01, 0.1, 1\}$, in Figures 25–27.

TABLE 13 Maximum error, ε_{max}, between analytical and Crank–Nicholson matrix solutions with $N = 100$, $M = 495$ and its associated position

Pe \ *Da*	**0.01**	**0.1**	**1**	**10**	**100**
0.01	$1.63 \cdot 10^{-3}$ [1, 1]	$1.52 \cdot 10^{-3}$ [1, 1]	$1.07 \cdot 10^{-3}$ [1, 1]	$2.70 \cdot 10^{-2}$ [4, 1]	$1.82 \cdot 10^{-2}$ [44, 1]
0.1	$4.44 \cdot 10^{-3}$ [1, 1]	$4.12 \cdot 10^{-3}$ [1, 1]	$3.04 \cdot 10^{-3}$ [1, 1]	$1.28 \cdot 10^{-3}$ [1, 1]	$5.99 \cdot 10^{-4}$ [0, 1]
1	$1.09 \cdot 10^{-2}$ [1, 1]	$9.92 \cdot 10^{-3}$ [1, 1]	$6.55 \cdot 10^{-3}$ [1, 1]	$6.28 \cdot 10^{-3}$ [0, 1]	$6.28 \cdot 10^{-3}$ [0, 1]
10	$6.14 \cdot 10^{-2}$ [0, 1]	$6.14 \cdot 10^{-2}$ [0, 1]	$6.14 \cdot 10^{-2}$ [0, 1]	$6.14 \cdot 10^{-2}$ [0, 1]	$6.14 \cdot 10^{-2}$ [0, 1]

TABLE 14 Maximum error, ε_{max}, between analytical and MOL matrix solutions with $N = 200$ and its associated position

Pe \ *Da*	**0.01**	**0.1**	**1**	**10**	**100**
0.01	$2.32 \cdot 10^{-5}$ [0, 1]	$2.32 \cdot 10^{-5}$ [0, 1]	$2.32 \cdot 10^{-5}$ [0, 1]	$2.68 \cdot 10^{-5}$ [5, 1]	$1.82 \cdot 10^{-5}$ [48, 1]
0.1	$2.66 \cdot 10^{-4}$ [0, 1]	$2.66 \cdot 10^{-4}$ [0, 1]	$2.66 \cdot 10^{-4}$ [0, 1]	$2.66 \cdot 10^{-4}$ [0, 1]	$2.66 \cdot 10^{-4}$ [0, 1]
1	$2.98 \cdot 10^{-3}$ [0, 1]	$2.98 \cdot 10^{-3}$ [0, 1]	$2.98 \cdot 10^{-3}$ [0, 1]	$2.98 \cdot 10^{-3}$ [0, 1]	$2.98 \cdot 10^{-3}$ [0, 1]
10	$3.11 \cdot 10^{-2}$ [0, 1]	$3.11 \cdot 10^{-2}$ [0, 1]	$3.11 \cdot 10^{-2}$ [0, 1]	$3.11 \cdot 10^{-2}$ [0, 1]	$3.11 \cdot 10^{-2}$ [0, 1]

TABLE 15 Maximum error, ε_{max}, between analytical and Crank–Nicholson matrix solutions with $N = 200$, $M = 495$ and its associated position

Pe \ *Da*	**0.01**	**0.1**	**1**	**10**	**100**
0.01	$1.67 \cdot 10^{-3}$ [1, 1]	$1.55 \cdot 10^{-3}$ [1, 1]	$1.10 \cdot 10^{-3}$ [4, 1]	$2.70 \cdot 10^{-2}$ [4, 1]	$1.82 \cdot 10^{-2}$ [42, 1]
0.1	$4.73 \cdot 10^{-3}$ [1, 1]	$4.41 \cdot 10^{-3}$ [1, 1]	$3.32 \cdot 10^{-3}$ [1, 1]	$1.53 \cdot 10^{-3}$ [1, 1]	$3.32 \cdot 10^{-4}$ [1, 1]
1	$1.33 \cdot 10^{-2}$ [1, 1]	$1.23 \cdot 10^{-2}$ [1, 1]	$8.69 \cdot 10^{-3}$ [1, 1]	$3.30 \cdot 10^{-3}$ [1, 1]	$2.98 \cdot 10^{-3}$ [0, 1]
10	$3.11 \cdot 10^{-2}$ [0, 1]	$3.11 \cdot 10^{-2}$ [0, 1]	$3.11 \cdot 10^{-2}$ [0, 1]	$3.11 \cdot 10^{-2}$ [0, 1]	$3.11 \cdot 10^{-2}$ [0, 1]

Graphically, there exists a similar behavior among the three employed methods not only for the *Pe* and *Da* values used for the simulation in these figures, but for all the *Pe* and *Da* values used in this paper. Nevertheless, it is more accurate to compare the three methods in a mathematical way.

Two kind of mathematical errors have been calculated, comparing analytical and numerical solution. Firstly, the maximum error, ε_{max}, between the analytical solution and each one of the numerical method employed has been found and also the time and spatial position where this error is reached; and secondly, the least-square error, $\varepsilon_{leastsq}$, is found. The main purpose of these measures is to find the adequate number of spatial slices, N, for achieving a good approximation between the dimensionless concentration matrix obtained by analytical or numerical methods. And, furthermore, to conclude which of the numerical solution is closer to the analytical one.

The first error is measured by calculating the maximum difference, in absolute value, between the dimensionless concentration matrix of the analytical solution, $A_{analytical}$, and the dimensionless concentration matrix of the numerical associated method, A_{method}. Remember that $A_{analytical}$ is defined in (15) with the suitable number of terms in the Fourier development seen in Table 3. The size of both matrices is 100×101 in this paper.

$$\varepsilon_{max} = \max(\max(\left|A_{analytical} - A_{method}\right|)). \tag{29}$$

Results can be seen in Tables 12 and 13. In these tables, when the ε_{max} is obtained, the position of the matrix element where this error occurs is indicated. The first index is the time node, n, and the second one is the spatial node, j, in the grid of the numerical methods.

It can be detected in general terms, in Tables 12 and 13, that at the initial time ($\theta = 0$) and the reactor inlet ($Z = 0$) is where the maximum value of ε_{max} is achieved in both methods. On the other hand, Crank–Nicholson's method produces greater errors than MOL. For $Da \leq 1$, ε_{max} increases as *Pe* increases. Nevertheless, for $Da \geq 10$, ε_{max} shows a minimum as *Pe* increases, independently of the numerical method used for calculating the dimensionless concentration. The following step is to increase the number of slices in the spatial domain, N, for trying to reduce ε_{max}.

TABLE 16 Maximum error, ε_{max}, between analytical and Crank–Nicholson matrix solutions with $N = 500$, $M = 495$ and its associated position

Pe \ Da	0.01	0.1	1	10	100
0.01	$1.69 \cdot 10^{-3}$ [1, 1]	$1.57 \cdot 10^{-3}$ [1, 1]	$1.12 \cdot 10^{-3}$ [1, 1]	$2.70 \cdot 10^{-2}$ [4, 1]	$1.82 \cdot 10^{-2}$ [40, 1]
0.1	$4.92 \cdot 10^{-3}$ [1, 1]	$4.60 \cdot 10^{-3}$ [1, 1]	$3.51 \cdot 10^{-3}$ [1, 1]	$1.70 \cdot 10^{-3}$ [1, 1]	$4.61 \cdot 10^{-4}$ [1, 1]
1	$1.51 \cdot 10^{-2}$ [1, 1]	$1.40 \cdot 10^{-2}$ [1, 1]	$1.03 \cdot 10^{-2}$ [1, 1]	$4.61 \cdot 10^{-3}$ [1, 1]	$9.94 \cdot 10^{-4}$ [0, 1]
10	$2.94 \cdot 10^{-2}$ [1, 1]	$2.53 \cdot 10^{-2}$ [1, 1]	$2.07 \cdot 10^{-2}$ [1, 1]	$1.20 \cdot 10^{-2}$ [0, 1]	$1.20 \cdot 10^{-2}$ [0, 1]

TABLE 17 Least-square error, $\varepsilon_{leastsq}$, between analytical and MOL matrix solutions with $N = 100$

Pe \ Da	0.01	0.1	1	10	100
0.01	$3.22 \cdot 10^{-13}$	$3.22 \cdot 10^{-13}$	$3.32 \cdot 10^{-13}$	$1.22 \cdot 10^{-4}$	$3.96 \cdot 10^{-5}$
0.1	$3.59 \cdot 10^{-11}$	$3.59 \cdot 10^{-11}$	$3.72 \cdot 10^{-11}$	$4.63 \cdot 10^{-11}$	$5.88 \cdot 10^{-11}$
1	$3.93 \cdot 10^{-9}$	$3.93 \cdot 10^{-9}$	$4.00 \cdot 10^{-9}$	$4.77 \cdot 10^{-9}$	$9.37 \cdot 10^{-9}$
10	$3.76 \cdot 10^{-7}$	$3.76 \cdot 10^{-7}$	$3.77 \cdot 10^{-7}$	$4.03 \cdot 10^{-7}$	$1.24 \cdot 10^{-6}$

TABLE 18 Least-square error, $\varepsilon_{leastsq}$, between analytical and Crank–Nicholson matrix solutions with $N = 100$, $M = 495$

Pe \ Da	0.01	0.1	1	10	100
0.01	$6.26 \cdot 10^{-9}$	$5.05 \cdot 10^{-9}$	$2.07 \cdot 10^{-9}$	$1.22 \cdot 10^{-4}$	$3.96 \cdot 10^{-5}$
0.1	$1.89 \cdot 10^{-8}$	$1.54 \cdot 10^{-8}$	$6.52 \cdot 10^{-9}$	$7.29 \cdot 10^{-10}$	$6.76 \cdot 10^{-11}$
1	$5.07 \cdot 10^{-8}$	$4.09 \cdot 10^{-8}$	$1.74 \cdot 10^{-8}$	$5.59 \cdot 10^{-9}$	$9.40 \cdot 10^{-9}$
10	$3.86 \cdot 10^{-7}$	$3.81 \cdot 10^{-7}$	$3.78 \cdot 10^{-7}$	$4.03 \cdot 10^{-7}$	$1.24 \cdot 10^{-6}$

TABLE 19 Least-square error, $\varepsilon_{leastsq}$, between analytical and MOL matrix solutions with $N = 200$

Pe \ Da	0.01	0.1	1	10	100
0.01	$5.40 \cdot 10^{-14}$	$5.39 \cdot 10^{-14}$	$5.40 \cdot 10^{-14}$	$1.22 \cdot 10^{-4}$	$3.96 \cdot 10^{-5}$
0.1	$7.01 \cdot 10^{-12}$	$7.01 \cdot 10^{-12}$	$7.09 \cdot 10^{-12}$	$7.66 \cdot 10^{-12}$	$8.47 \cdot 10^{-12}$
1	$8.83 \cdot 10^{-12}$	$8.83 \cdot 10^{-10}$	$8.88 \cdot 10^{-10}$	$9.36 \cdot 10^{-10}$	$1.24 \cdot 10^{-9}$
10	$9.61 \cdot 10^{-8}$	$9.62 \cdot 10^{-8}$	$9.62 \cdot 10^{-8}$	$9.79 \cdot 10^{-8}$	$1.59 \cdot 10^{-7}$

If Tables 14 and 15 are compared, it can be seen that MOL always generates dimensionless concentrations closer to the analytical ones than Crank–Nicholson for the studied values of *Péclet* and *Damköhler*. And the highest ε_{max} remains at the initial time and reactor inlet for both numerical methods. Furthermore, if we compare these tables with Tables 12 and 13, it can be clearly seen that for $N = 200$, ε_{max} increases with *Pe* using MOL, for all the *Da* values studied. However, this fact is not as clear as Crank–Nicholson where the relation of ε_{max} with *Pe* and *Da* values does not change when N increases from 100 to 200. Table 16 shows that, for the Crank–Nicholson's method, ε_{max} is not reduced to significant levels even taking $N = 500$; therefore, these new calculations for these great values of N will not be considered.

It is interesting to remark that ε_{max} only shows the point where the difference between analytical and numerical solutions is the greatest, but it can be an isolated point. For avoiding this fact, the least-square error, $\varepsilon_{leastsq}$, is calculated according to (30). This error takes into account all the points in the dimensionless matrix concentration calculated by analytical and numerical methods, instead of only the most unfavorable point.

$$\varepsilon_{leastsq} = \frac{\sum_{j,n}\left[A_{analytical}(j,n) - A_{method}(j,n)\right]^2}{101 \times 100}. \tag{30}$$

If the least-square approximation is used for calculating an error between the numerical and analytical solution, Tables 17 and 18 are obtained.

From Tables 17 and 18, a similar behavior is deduced between ε_{max} and $\varepsilon_{leastsq}$ with $N = 100$. So Crank–Nicholson's method generates greater errors than MOL. Also, for $Da <= 1$, $\varepsilon_{leastsq}$ increases with *Pe* and for $Da >= 10$, it shows a minimum as *Pe* increases, regardless of the numerical method used. If the number of spatial slices increases to $N = 200$, Tables 19 and 20 are obtained.

TABLE 20 Least-square error, $\varepsilon_{leastsq}$, between analytical and Crank–Nicholson matrix solutions with $N = 200$, $M = 495$

Pe \ *Da*	**0.01**	**0.1**	**1**	**10**	**100**
0.01	$6.37 \cdot 10^{-9}$	$5.15 \cdot 10^{-9}$	$2.14 \cdot 10^{-9}$	$1.22 \cdot 10^{-4}$	$3.96 \cdot 10^{-5}$
0.1	$2.09 \cdot 10^{-8}$	$1.72 \cdot 10^{-8}$	$7.63 \cdot 10^{-9}$	$9.59 \cdot 10^{-10}$	$2.95 \cdot 10^{-11}$
1	$6.88 \cdot 10^{-8}$	$5.60 \cdot 10^{-8}$	$2.34 \cdot 10^{-8}$	$3.03 \cdot 10^{-9}$	$1.26 \cdot 10^{-9}$
10	$1.51 \cdot 10^{-7}$	$1.31 \cdot 10^{-7}$	$1.14 \cdot 10^{-7}$	$9.92 \cdot 10^{-8}$	$1.59 \cdot 10^{-7}$

TABLE 21 Least-square error, $\varepsilon_{leastsq}$, between analytical and Crank–Nicholson matrix solutions with $N = 400$, $M = 495$

Pe \ *Da*	**0.01**	**0.1**	**1**	**10**	**100**
0.01	$6.45 \cdot 10^{-9}$	$5.22 \cdot 10^{-9}$	$2.19 \cdot 10^{-9}$	$1.22 \cdot 10^{-4}$	$3.96 \cdot 10^{-5}$
0.1	$2.28 \cdot 10^{-8}$	$1.89 \cdot 10^{-8}$	$8.72 \cdot 10^{-9}$	$1.29 \cdot 10^{-9}$	$4.67 \cdot 10^{-11}$
1	$9.50 \cdot 10^{-8}$	$7.88 \cdot 10^{-8}$	$3.57 \cdot 10^{-8}$	$4.74 \cdot 10^{-9}$	$2.78 \cdot 10^{-10}$
10	$1.76 \cdot 10^{-7}$	$1.28 \cdot 10^{-7}$	$8.73 \cdot 10^{-8}$	$3.08 \cdot 10^{-8}$	$2.74 \cdot 10^{-8}$

TABLE 22 Least-square error, $\varepsilon_{leastsq}$, between analytical and Crank–Nicholson matrix solutions with $N = 500$, $M = 495$

Pe \ *Da*	**0.01**	**0.1**	**1**	**10**	**100**
0.01	$6.75 \cdot 10^{-9}$	$1.93 \cdot 10^{-8}$	$1.30 \cdot 10^{-7}$	$1.22 \cdot 10^{-4}$	$3.96 \cdot 10^{-5}$
0.1	$2.35 \cdot 10^{-8}$	$3.32 \cdot 10^{-8}$	$1.38 \cdot 10^{-7}$	$2.13 \cdot 10^{-8}$	$3.86 \cdot 10^{-10}$
1	$1.04 \cdot 10^{-7}$	$9.96 \cdot 10^{-8}$	$1.85 \cdot 10^{-7}$	$3.41 \cdot 10^{-8}$	$1.30 \cdot 10^{-9}$
10	$2.10 \cdot 10^{-7}$	$1.61 \cdot 10^{-7}$	$3.17 \cdot 10^{-7}$	$9.62 \cdot 10^{-8}$	$2.00 \cdot 10^{-8}$

Lower values for the $\varepsilon_{leastsq}$ are clearly obtained for MOL when N increases from 100 to 200. Nevertheless, this effect is not shown for Crank–Nicholson's method, where the $\varepsilon_{leastsq}$ even increases in some cases when N raises to 200. Using higher values for N as 400, Table 21, or 500, Table 22, in Crank–Nicholson's method does not reduce $\varepsilon_{leastsq}$ in comparison with $N = 100$, but increases the computation time.

So it is enough to apply MOL with $N = 100$ in the spatial domain, while Crank–Nicholson's method with the same number of slices gives worse approximations. In view of these numerical results, the authors have been taken $N = 100$ for MOL, and even if the value of N is increased, there is no significant improvement in the results of the least-square error, $N = 100$ and $M = 495$ for the Crank–Nicholson's method.

All of this leads us to conclude that, in general, for the convection–diffusion–reaction equation with Danckwerts boundary conditions, MOL approximates better than Crank–Nicholson to the analytical solution with the particular values here exposed, $C_{Ae} = 1\,\text{mol/m}^3$, $C_{A0} = 0\,\text{mol/m}^3$.

6 | CONCLUSIONS

The convection–diffusion–reaction PDE with Danckwerts boundary conditions applied in a tubular reactor has been solved using three different techniques: one analytical solution and two numerical methods. The numerical approximations employed are based on different strategies, because MOL discretizes the dimensionless PDE only in the spatial domain, generating an ODE system, while Crank–Nicholson's method discretizes the PDE in both spatial and time domains, resulting an algebraic equations system.

When the analytical technique is taken, Fourier expansion appears after transforming the PDE into a heat equation with non-homogeneous boundary conditions, through the application of two changes of variables, and solving by separation of variables. The number of terms to consider in this developments is important in order to control the solution precision (i.e., below 10^{-4}), and it depends on the values of *Péclet* number in a direct correlation way. The other dimensional-less parameter, *Damköhler* number, does not have a relevant transcendence, as it has been demonstrated in the paper.

Stability of both numerical methods has been studied in this work. Stability of MOL depends on the relationship between discretization time and spatial steps. Although the steps applied in this paper do not meet the stability criterion for fixed-step ODE solvers, the stability is assured using a variable-step solver (`ode15s`) regardless the values of *Pe* and *Da* used in the simulations with MOL. On the other hand, in this paper, the stability of Crank–Nicholson's method has been demonstrated for all the conditions studied. Nevertheless, some oscillations appear with Crank–Nicholson's method, depending on the values of *Pe* and *Da* applied. These oscillations are eliminated simply increasing the number of slices used in the time domain discretization.

The graphical comparison between the analytical dimensionless concentrations and those calculated by both numerical methods shows a good approximation, and it is very difficult to distinguish them with the naked eye. So a mathematical comparison has been established by means of two errors: ε_{max} and $\varepsilon_{leastsq}$. On one hand, ε_{max} shows the maximum difference between analytical and numerical solutions for MOL and Crank–Nicholson and the point of the time and spatial grid where this maximum occurs. On the other hand, $\varepsilon_{leastsq}$ compares analytical and numerical solutions considering all the points along the time and space domains.

The maximum value of ε_{max} is detected, in general, at the initial time and reactor inlet for both numerical methods, although Crank–Nicholson's method produces greater errors than MOL, regardless of the number of slices used in the spatial domain, N. When $\varepsilon_{leastsq}$ is used, it can be checked that Crank–Nicholson's method also generates greater errors than MOL. Moreover, increasing N reduces clearly this error for MOL, but this behavior is not detected with Crank–Nicholson's method.

It can be concluded that MOL approximates better to the analytical solution than Crank–Nicholson for the convection–diffusion–reaction equation with Danckwerts boundary conditions, using a lower number of slices in the spatial domain and reducing the computational effort needed.

All the routines here used have implemented with Matlab R2020b. In CPU: Processor: Intel (R) Core (TM) i7-6700 K CPU @ 4.00 GHz. Memory (RAM) 16.0 GB. 64-bit operating system, x64 processor. The average time elapsed in the execution of the programs has been:

- MOL program: 0.3 s
- Crank–Nicholson's method: 0.4 (using Gaussian algorithm for solving the algebraic linear system) or 0.03 s (using Thomas algorithm)
- Analytical solution: 30 min for 200 terms, 90 min for 300 terms, 2 h for 600 terms, and 7 h for 1800 terms

ACKNOWLEDGEMENT

There are no funders to report for this submission.

NOMENCLATURE

A_N	matrix of analytical concentrations
$C_A(z,t)$	concentration of A (mol/m^3)
C_{A0}	initial concentration of component A (mol/m^3)
C_{Ae}	concentration of component A at the reactor inlet (mol/m^3)
$C_{An}(Z,\theta)$	normalized concentration, $C_{An}(Z,\theta) = \frac{C_A(z,t)}{C_{Ae}}$
C_j	$C_j = C_{An}(Z_j,\theta)$
C_j^n	$C_j^n = C_{An}(Z_j,\theta_n)$
Da	Damköhler number, $Da = \frac{k_A L}{v_z}$
D_A	diffusion coefficient of component A (m^2/s)
h	spatial step
j	spatial subindex, $j = 1, \ldots, N+1$
k	time step
k_A	kinetic rate constant (s^{-1})
L	reactor length (m)
M	number of slices in time grid
n	time superindex, $n = 0, \ldots, M$
N	number of slices in spatial grid or number of terms to consider in Fourier expansions
Pe	Péclet number, $Pe = \frac{v_z L}{D_A}$
r	$r = \frac{Pe}{2}$
s	$s = \frac{Pe}{4} + Da$
t	time variable (s), t$\in [0, +\infty)$
T_n	eigenfunctions of analytical solution in time domain
TOL	tolerance considered for the number of terms in the Fourier expansions, $TOL = \max(\max(\lvert A_{N+100} - A_N \rvert))$

v_z	fluid velocity in the z spatial direction (m/s)
X_n	eigenfunctions of analytical solution in spatial domain
z	spatial variable (m), $z \in [0, L]$
Z	dimensionless spatial variable, $Z \in [0, 1]$
λ_n	eigenvalues of analytical solution
θ	dimensionless time variable, $\theta \in [0, +\infty)$

CONFLICT OF INTEREST

This work does not have any conflicts of interest.

ORCID

Lucía Agud Albesa https://orcid.org/0000-0002-1222-7988

REFERENCES

1. Golz WJ, Dorroh JR. The convection-diffusion equation for a finite domain with time varying boundaries. *Appl Math Lett*. 2001;14:983-988.
2. Mohammadi A, Manteghian M, Mohammadi A. Numerical solution of One-dimensional advection-diffusion equation Using simultaneously temporal and spatial weighted parameters. *Australian J Basics Appl Sci*. 2011;5(6):1536-1543.
3. Jiménez Zenteno JR. Una solución analítica para la ecuación de difusión advección reacción por medio de series de Fourier. *Matemática, Educación e Internet*. 2018;18(2):1-15.
4. Polyanin AD, Nazaikinskii VE. *Handbook of Linear Partial Differential Equations for Engineers and Scientist*. CRC Press Taylor & Francis Group LLC; 2016.
5. van Genuchten MT, Alves WJ. *Analytical Solutions of the One-Dimensional Convective-Dispersive Solute Transport Equation*, U.S. Department of Agriculture, Agricultural Research Service Technical Bulletin, vol. 1661: Government Printing Office; 1982.
6. Bandopadhyay A, Le Borgne T, Méheust Y, Dentz M. Enhanced reaction kinetics and reactive mixing scale dynamics in mixing fronts under shear flow for arbitrary Damköhler numbers. *Adv Water Resour*. 2017;100:78-95.
7. Yadav RR, Jaiswal DK, Yadav HK, Rana GU. One-dimensional temporally dependent advection-dispersion equation in porous media: analytical solution. *Nat Resour Model*. 2010;23(4):521-539.
8. Haberman R. *Ecuaciones en Derivadas Parciales con Series de Fourier y Problemas de Contorno*. Prentice Hall. Pearson Education, S.A.; 2003.
9. Olsen-Kettle L. *Numerical Solution of Partial Differential Equations*. Centre for Geoscience Computing, School of Earth Sciences, University of Queensland; 2011.
10. Vande Wouwer A, Saucez W, Schiesser E. Simulation of distributed parameter systems using a Matlab based method of lines toolbox: chemical engineering applications. *Ind Eng Chem Res*. 2004;43(14):3469-3477.
11. David R, Saucez P, Vasel JL, Wouwer AV. Modelling and numerical simulation of secondary settlers: a method of lines strategy. *Water Res*. 2009;43(2):319-330.
12. Vande Wouwer A, Saucez P, Schiesser WE. *Adaptive Method of Lines*. Chapman Hall/CRC Press; 2001. Available online at CRC Press: www.mathnetbase.com edition.
13. Hangos KM, Cameron I. *Process Modelling and Model Analysis*. Academic Press; 2001.
14. Lozada-Cruz G, Rubio-Mercedes CE, Rodrigues-Ribeiro J. Numerical Solution of Heat Equation with. *Tendencias em Matemà,tica Aplicada e Computacional*. 2018;19(2):209-220. doi:10.5540/tema.2018.019.02.0209
15. Dlotko T. *Certain Methods of Proving Existence and Uniqueness in PDE Theory*. Silesian University. http://www.math.us.edu.pl/sdoktor/pde_eu.pdf (Last visit: December 2021).
16. Crespo M, Ivorra B, Ramos AM. Asymptotic stability of a coupled advection-diffusion-reaction system arising in bioreactor processes. *Electron J Differ Equ*. 2017;194:1-26. http://ejde.math.txstate.edu or http://ejde.math.unt.edu
17. Dramé AK. A semilinear parabolic boundary-value problem in bioreactors theory. *Electron J Differ Equ*. 2004;129:1-13. http://ejde.math.txstate.edu or http://ejde.math.unt.edu
18. Kalli K, Soltanov KN. Existence and behavior of solutions for convection-diffusion equations with third type boundary conditions. *TWMS J Pure Appl Math*. 2017;8(2):209-222.
19. Ziskind G, Shmueli H, Gitis V. An analytical solution of the convection-dispersion-reaction equation for a finite region with a pulse boundary condition. *Chem Eng J*. 2011;167(1):403-408. doi:10.1016/j.cej.2010.11.047
20. Vande Wouwer A. *Simulation of ODE/PDE Models with Matlab, OCTAVE and SCILAB. Scientific Engineering Applications*. Springer; 2014.
21. Ross KA. *Elementary Analysis: The Theory of Calculus*. Springer-Verlag, N.Y., Inc.; 1980.
22. de Burgos Roman J. *Cálculo Infinitesimal de una Variable*. McGraw-Hill/Interamericana de España S.A.; 1994.

23. de Frutos J. Estabilidad y convergencia de esquemas numéricos para sistemas de Dirac no lineales. *Revista Internacional de Mé,todos Numéricos para Cálculo y Diseño en Ingeniería*. 1989;5(2):185-202.
24. Zuazua E. Métodos numéricos para la resolución de ecuaciones en derivadas parciales. (Source: http://www.bcamath.org/documentos-public/archivos/personal/comites/notas-05-065-complete.pdf); 2009.
25. Sauer T. Análisis Numérico, 2nd ed. Pearson; 2013.
26. Mathews JH, Fink KD. *Métodos Numéricos con Matlab*. 3rd ed. Prentice Hall; 1999.
27. https://www.sfu.ca/~rjones/bus864/notes/notes2.pdf (visited by last time January 20, 2021).
28. Abbaszadeh M, Dehghan M. A POD-based reduced-order Crank-Nicolson/fourth-order alternating direction implicit (ADI) finite difference scheme for solving the two-dimensional distributed-order Riesz space-fractional diffusion equation. *Appl Numer Math*. 2020;158:271-291. doi:10.1016/j.apnum.2020.07.020
29. Carranza M. *Tratamiento numérico y Aplicación de la Ecuación de Advección Difusión, Tesina (Lic.)*. Universidad Nacional Mayor de San Marcos (Lima), Facultad de Ciencias Matemáticas Escuela Académico Profesional de Matemática; 2009. https://hdl.handle.net/20.500.12672/12789
30. Jeong D, Libao Y, Lee C, Yang J, Choi Y, Kim J. Verification of convergence rates of numerical solutions for parabolic equations. *Math Probl Eng*. 2019;2019:10. doi:10.1155/2019/8152136

How to cite this article: Agud Albesa L, Boix García M, Pla Ferrando ML, Cardona Navarrete SC. A study about the solution of convection–diffusion–reaction equation with Danckwerts boundary conditions by analytical, method of lines and Crank–Nicholson techniques. *Math Meth Appl Sci*. 2023;46(2):2133-2164. doi:10.1002/mma.8633